N72- 25917
RF Project 2601
Final Report

THE OHIO STATE UNIVERSITY

RESEARCH FOUNDATION

1314 KINNEAR ROAD COLUMBUS, OHIO 43212

RADIATIVE TRANSFER EFFECTS BEHIND REFLECTED SHOCK WAVES

Robert M. Nerem

1 March 1968 - 28 February 1972

NATIONAL AERONAUTICAL AND SPACE ADMINISTRATION
Washington D. C.

Grant # NGL-36-008-106

RF Project 2601

Report No. 13

FINAL

REPORT

By

THE OHIO STATE UNIVERSITY
RESEARCH FOUNDATION

1314 KINNEAR RD.
COLUMBUS, OHIO 43212

To NATIONAL AERONAUTICAL AND SPACE ADMINISTRATION

Washington D. C. 20546

Grant No. NGL-36-008-106

On RADIATIVE TRANSFER EFFECTS BEHIND

REFLECTED SHOCK WAVES

For the period 1 March 1968 - 28 February 1972

Submitted by Robert M. Nerem

Department of Aeronautical and Astronautical Engineering

Date 13 March 1972

ABSTRACT

During the period March 1, 1968 - February 29, 1972 the Aeronautical and Astronautical Research Laboratory at The Ohio State University carried out an investigation of radiative transfer effects behind reflected shock waves in air and nitrogen. The theoretical studies largely centered on the nonequilibrium coupling of collisional, ionization, and radiative transfer processes behind reflected shock waves in nitrogen. Experimental studies included broad-band photomultiplier radiative intensity measurements, luminosity photographs of the reflected shock wave front, end-wall heat transfer measurements, and reflected shock velocity time-history measurements. This report summarizes the results of these activities and discusses comparisons between the theoretical and experimental results.

ACKNOWLEDGMENT

This report is a summary of a combined theoretical and experimental investigation of radiative transfer effects behind reflected shock waves in air and nitrogen which has been conducted by the Aeronautical and Astronautical Research Laboratory of the Department of Aeronautical and Astronautical Engineering at The Ohio State University.

This work was sponsored by the National Aeronautics and Space Administration under Grant NGL 36-008-106 and carried out during the period March 1, 1968 to February 29, 1972.

The author is indebted to the following persons for their participation in this effort and their contribution to the results obtained: J. B. Bader, L. A. Carlson, G. L. Geiger, R. A. Golobic, and R. C. Prior.

TABLE OF CONTENTS

LIST OF FIGURES

I. INTRODUCTION

During recent years there has been a continuing interest in investigating the transport of energy in high temperature gases through the emission and absorption of radiation. Much of this work has been devoted to the study of the radiative processes and in such studies the shock tube has played an important role.

However, more recently there has been an increasing interest in the coupling of radiative and conductive transport in high temperature gases through the effects of self-absorption and radiative cooling. Much of the resulting activity has been motivated by the importance of the contribution of shock layer radiation to heat transfer to space vehicles during atmospheric entry. Calculations of stagnation point radiative heat transfer and of the structure of the blunt body radiating shock layer have thus been carried out; however, with the exception of shock tube studies of the spectral and integrated emission characteristics of high temperature gases and of similar studies in ballistic ranges (in both of which radiative cooling, in general, has not been an important factor), there have been virtually no experiments which would complement these theoretical studies of radiative gasdynamic coupling.

The present research effort was thus motivated by a desire to investigate a problem in radiative gasdynamics in which the radiative transfer was an important, if not the dominant mode of energy transport, and which at the same time lent itself to both theoretical and experimental investigation. One such problem is that of the reflection of a planar shock wave from an isothermal wall. Theoretically, the reflected shock problem is attractive because it is one-dimensional and the integro-differential nature of the energy equation in the presence of radiative transfer is thus more amendable to solution. From an experimental viewpoint, on the other hand, such a reflection process may be studied in a shock tube. In particular, in an arc-driven shock tube such as is available at The Ohio State University, conditions may be created in which the end-wall heat transfer is radiation dominated.

It should be noted that although the one-dimensional, unsteady flow problem of the reflection of a planar shock wave from the end wall of a shock tube is fundamentally different from the problem of steady state flow at the stagnation point of a blunt body, certain similarities still do exist. This is particularly true in terms of the surface heat transfer and may best be seen by comparing the two problems for a transparent, radiating gas in which there is no radiative cooling. For this case, the dependence of both the end-wall heat transfer and the stagnation point heat transfer rates are shown in Table 1. It may be seen that t, the time after shock reflection, plays the same role in the end-wall heat transfer problem that R, the nose radius, does in the stagnation point problem. Both R and t, in their respective problems, are related to the shock layer thickness and the analogous role of the two variables is not surprising. However, it would be only fortuitous if these two problems, in general, were identical in terms of R and t since they are fundamentally different problems.

Table 1. Comparison Between Heat Transfer Dependence in End-Wall and Stagnation-Point Problems

	Radiative Heat Transfer	Convective (Conductive) Heat Transfer
End Wall Problem	$q_R \propto t$	$q_c \propto t^{-1/2}$
Stagnation Point Problem	$q_R \propto R$	$q_c \propto R^{-1/2}$

It should be emphasized that the purpose for establishing such an approximate analogy between the end-wall heat transfer problem and the stagnation-point problem is that the former problem may be readily studied in the laboratory. In particular, in an arc-driven shock tube post-reflected shock wave conditions can be produced in air for which radiation is the dominant energy transport mechanism. Furthermore, if simulation is based on the matching of the post-shock pressure and total enthalpy for the two problems of a reflected shock wave and the stagnation point of an entry vehicle, then flight velocities ranging as high as 18 km/sec and altitudes up to 60 km can be simulated.

It should also be noted that this effort has been a continuation of a study of radiative transfer effects behind reflected shock waves in air which has been in progress at The Ohio State University. These studies, which will be discussed further in the following section, had previously been limited to relatively high reflected shock pressures ranging from 10-20 atmospheres and, thus, correspond to conditions of local chemical and thermodynamic equilibrium. In order to simulate lower densities where nonequilibrium effects may be important, it is necessary to go to lower shock tube initial pressures. One of the key elements of this investigation has been to investigate radiative-gas dynamic coupling in the nonequilibrium reflected shock-heated gases at these lower pressures, and numerical calculations including radiative emission and absorption, two-temperature effects, and ionization nonequilibrium behind reflected shock waves in nitrogen are presented and discussed in Section III.

Finally, a number of experimental measurements have been carried out in The Ohio State University arc-driven shock tube facility as part of this effort. These experiments are discussed in Section IV; comparisons between theory and experiment are included in Section V. A summary of the publications resulting from the effort on this Grant is included in Appendix I.

II. RADIATIVE COOLING IN EQUILIBRIUM AIR

The reflection of a normal shock wave from a planar wall is shown schematically in Figure 1. Also shown are conditions behind both a strong incident shock wave and the associated reflected wave. These properties, which are typical of those attainable in an arc-driven shock tube, are for an incident shock wave moving at a velocity of 8.85 km/sec into air at an initial pressure of 1.0 torr and a temperature of 300°K. The indicated conditions are based on calculations using the conventional normal shock wave equations, the assumption of chemical and thermodynamic equilibrium, and the neglection of radiative transfer effects. Behind the incident shock wave, the gas is virtually completely dissociated, the pressure is on the order of 1 atmosphere, and chemical equilibration occurs within a distance of 1 cm of the shock front.

On the other hand, behind the reflected shock wave, ionization is important and an equilibrium electron density of approximately 2×10^{18} particles/cm^3 is attained. The reflected shock wave velocity U_{SR}, is 1.30 km/sec, while the flow velocity behind the incident wave is approximately 8 km/sec. Thus, even though in the presence of radiative cooling the reflected shock wave may attenuate as it moves away from the wall, the thermodynamic conditions immediately behind the reflected wave will be relatively unchanged since it is the flow ahead of the wave that primarily governs the reflected shock strength. It should be noted that, for the relatively high initial driven tube pressure of 1.0 torr, the pressure in the reflected shock wave region is on the order of 20 atmospheres. Thus, chemical equilibration is even more rapid here than behind the incident wave with near-equilibrium conditions being reached within a distance of 10^{-1} cm behind the reflected shock front.[3] Of course, at lower pressures nonequilibrium effects may be important and these will be discussed in the following section.

In considering the radiative properties of high temperature air, in the general temperature range of 10,000-20,000°K the important sources of radiation are due to both nitrogen and oxygen transitions and include: (i) visible and vacuum ultraviolet(VUV) recombination radiation; (ii) VUV, visible, and near infrared atomic lines; and (iii) bremsstrahlung emission. The ground state recombination (free-bound) radiative transitions, which occur around 1000Å and lower, are particularly strong, and in this wavelength region the gas will be optically thick once the reflected shock wave is more than 0.01 cm from the end wall. The VUV and near IR atomic lines are also self-absorbed; however, the visible continuum radiation is transparent.

A parameter which characterizes the influence of radiative transfer in a gasdynamic problem is the so-called radiation loss parameter, Γ, which may be defined for the present problem as

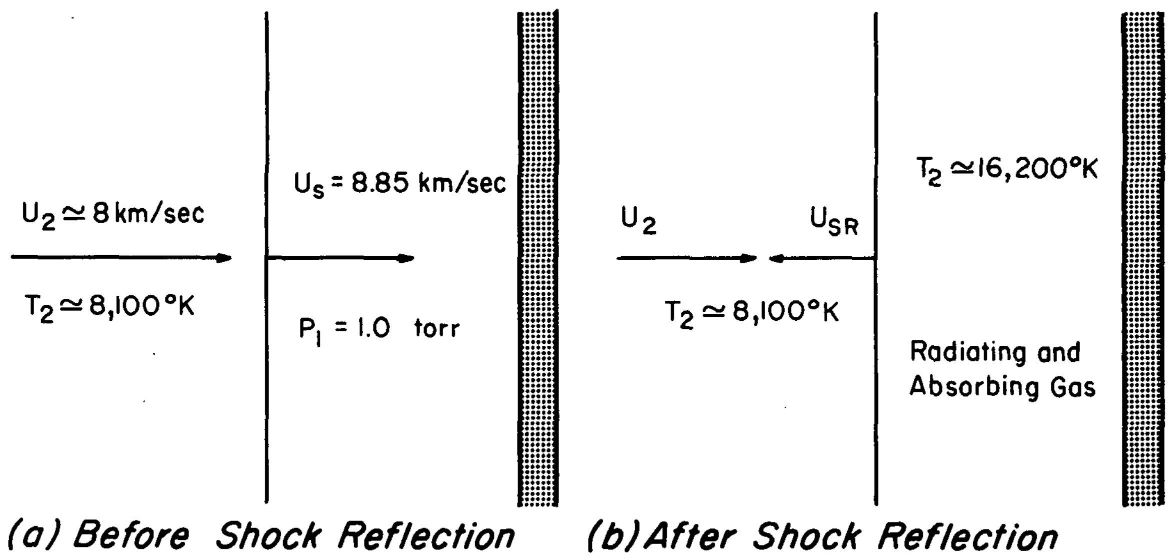

Figure 1 - Illustration of Shock Reflection Process for Typical Shock Tube Conditions in Air: (a) Before Shock Reflection; (b) After Shock Reflection

$$\Gamma = \frac{\dot{q}_R}{\rho_5 U_{SR} h_5} \qquad (1)$$

Here $\dot{q}_R$ is the total radiative flux away from the reflected shock region and the denominator is the energy flux through the reflected shock wave itself. If one considers the reflected shock region to be transparent (no absorption) and isothermal, then for an incident shock velocity of 8.85 km/sec, an initial pressure of $P_1 = 1.0$ torr, and a characteristic thickness of 1 cm, the loss parameter Γ will have a value in excess of 50. This value is somewhat unrealistic since the VUV continuum radiation is known to be strongly self-absorbed. However, even including self-absorption in evaluating $\dot{q}_R$ (for an isothermal slab), Γ will still have a value on the order of unity, and important cooling effects would be expected.

It should be noted that, for the conditions of Figure 1, approximately 100 kW/cm^2 of radiation is pouring out of the reflected shock front and passes through the gas upstream of the reflected wave. This gas, though moderately high in temperature and density, is rather transparent with the only exception being the VUV bound-free transitions. The upstream gas may be taken to be optically thick in this portion of the VUV region and the VUV blackbody flux for $\lambda \leq 0.11$ microns at a temperature corresponding to that of the reflected shock layer is approximately 5 kW/cm^2. Comparing this to the specific enthalpy flux of the upstream gas, which is approximately 185 kW/cm^2, it is apparent that the influence of upstream absorption on the thermodynamic state of that gas is small.

However, as indicated earlier, radiative transfer effects in the reflected shock region itself are important. This is true both in terms of self-absorption as well as radiative cooling; thus it is of interest to include radiative transfer in the actual solution of the equations governing the flow field and heat transfer behind a reflected shock wave. Unfortunately, any exact inclusion of radiative transfer is virtually impossible because of the complex nature of the spectral dependence of the absorption coefficient of most gases of interest. It is not that the radiative properties themselves cannot be calculated, but to include them in a nonisothermal, time-dependent flow field calculation would be extremely time consuming.

In order to include the effects of non-gray self-absorption, while at the same time avoiding the complexities of an exact inclusion of spectral absorption, a number of investigators have proposed the use of step-models for the absorption coefficient. In the use of these step-models for air, the far vacuum ultraviolet wavelength region (e.g., $\lambda < 0.11$-0.15 microns) has, in general, been highly absorbing, but with the visible and near infrared regions being relatively transparent. Such a model is a reasonable approximation to the continuum absorption coefficient for air at temperatures less than 20,000°K, but neglects important atomic line transitions.

To improve on such existing absorption coefficient models, a five-step model was developed as part of this effort for use in the temperature range of approximately 8-20,000°K.[4-5] This model corresponds to the range of interest not only in the present problem, but also in entry radiation calculations. The absorption coefficient model proposed for high temperature air calculations includes five regions as is illustrated in Figure 2 where the effective absorption cross section (based on the nitrogen atom number density) is shown as a function of wavelength. In the present analysis this model is based on nitrogen line and continuum transitions.

The details of this model are discussed in References 4 and 5; however, it should be noted that the temperature limitations on the proposed model are due to the fact that only transitions associated with nitrogen atoms have been included. Below 8-10,000°K, molecular band radiation becomes important, while above 18-20,000°K bound-bound, bound-free, and free-free transitions involving N^+ and N^{++} may be important. These transitions have not been included in the present results.

It should also be noted that while only nitrogen radiative transitions have been used in evaluating the absorption coefficients for the different regions of the step-model, from a practical viewpoint the results should also be applicable to air plasmas since nitrogen transitions dominate its radiative emission and absorption in the temperature range considered.

In order to test whether or not the present five-step model would be satisfactory for calculations of the integrated radiative intensity and heat flux in high temperature air, comparisons have been made between results obtained using the proposed model and both the shock tube data of Nerem and Stickford[7] and exact calculations provided by Wilson[8] of the Lockheed Palo Alto Research Laboratory. Satisfactory agreement has been shown to exist.

The five-step absorption coefficient model illustrated in Figure 2 thus represents a relatively simple approximation of the spectral characteristcs of nitrogen or air and yet appears to retain the necessary non-gray features (further discussion in Section V). However, with such a model one may then proceed to the problem of including radiative transfer effects in a numerical solution for the flow field and heat transfer behind a reflected shock wave in air.

Anderson[9] was the first to consider the influence of radiative transfer on the properties of a reflected shock wave in air. With the exception of his absorption coefficient model, the calculations to be presented in this section are quite similar (though not identical) to those of Anderson and, in fact, use a modification of his basic computer program. The major assumptions contained in the analysis from which results are presented here are: (1) the flow is one-dimensional,

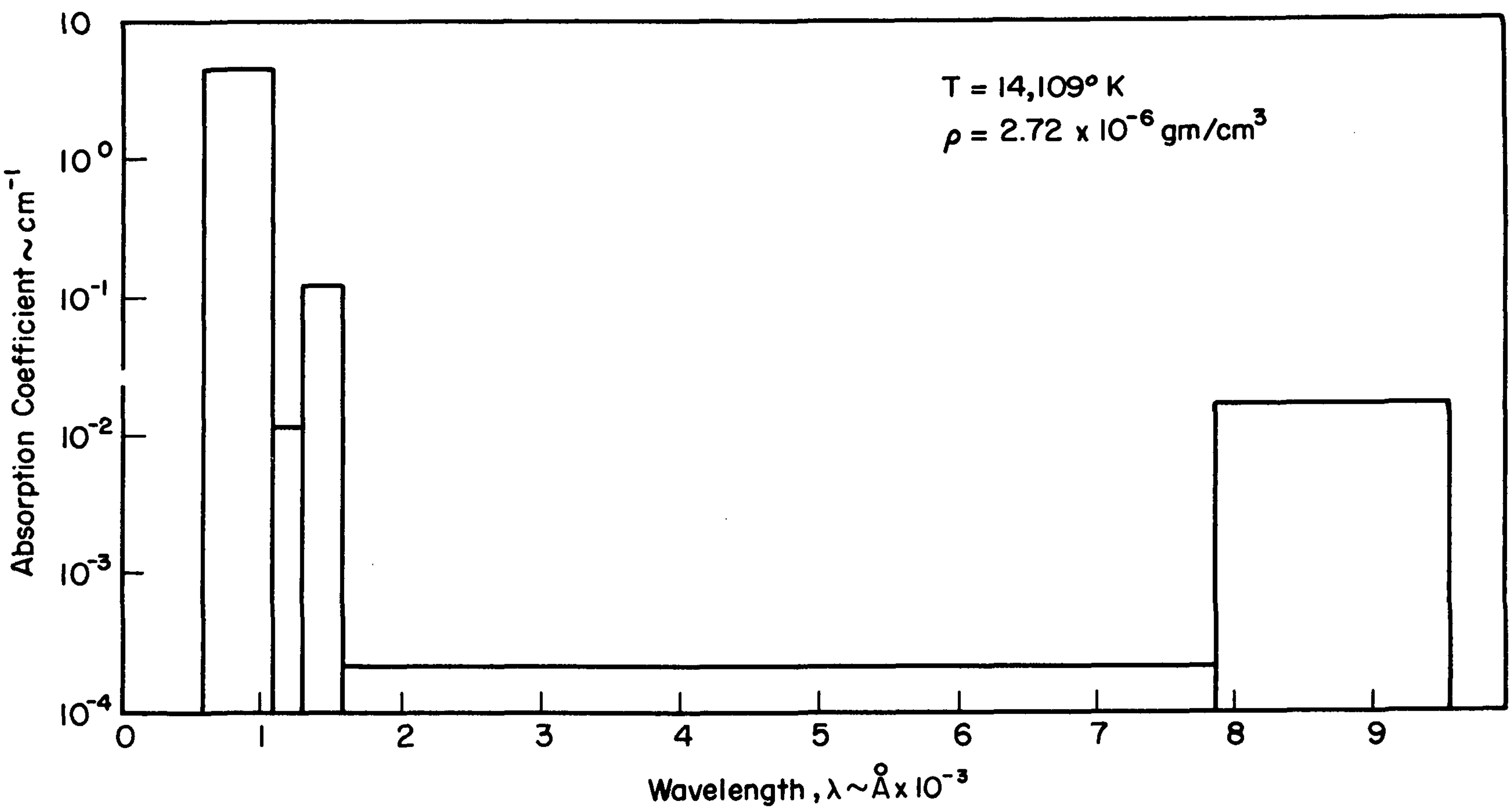

Figure 2 - Illustration of Five-Step Absorption Coefficient Model for Typical Reflected Shock Wave Conditions in Air

heat conducting, unsteady, and in local chemical and thermodynamic equilibrium; (2) the reflected shock wave is itself a discontinuity and moves in a uniform region of equilibrium air produced by the incident shock wave; (3) viscous dissipation and pressure gradient effects are negligible; (4) the gas between the end-wall and the reflected shock wave is emitting and self-absorbing with radiative properties given by a five-step model; and (5) the gas ahead of the reflected shock wave is nonemitting and nonabsorbing, while the end-wall from which the incident shock reflects is a cold blackbody and, thus, nonemitting and completely absorbing of all incident radiation. The thermodynamic and transport properties used were those for equilibrium air as calculated by Hansen[10] and correlated by Viegas and Howe.[11] A numerical forward finite difference method of solution has been used and the details of this solution are contained in References 5, 6, and 9.

The major portion of these calculations were carried out for incident shock waves moving into air at an initial pressure and temperature of 1.0 torr and 300°K. Incident shock wave velocities from 7 to 10 km/sec were considered. These velocities correspond to the range covered by shock tube experiments carried out as part of this effort; comparisons with existing data will be made in Section V. Additional calculations were also carried out at an initial driven tube pressure of 0.2 torr.

Selected results from these calculations are shown in Figures 3-6. Included are the time-histories of the shock layer temperature profile and end-wall heat transfer for two cases. The first case, results for which are shown in Figures 3 and 4, is an incident shock velocity of 9.2 km/sec in air at an initial driven tube pressure of 1.0 torr, and the second case, results for which are shown in Figures 5 and 6, is an incident shock velocity of 10 km/sec in air at an initial driven tube pressure of 0.2 torr. The fact that cooling is indeed present at these incident shock wave velocities is demonstrated by the calculated temperature profiles presented in Figures 3 and 5. As may be seen, radiative cooling accounts for a decrease in gas temperature on the order of 1000°K over a period of approximately 10 microseconds. Also shown is the effect of thermal conduction on the temperature profile in the immediate vicinity of the wall. However, for the high pressures of the present calculations, the end-wall thermal boundary layer is thin and the primary effect is cooling by radiation.

One of the characteristics of the reflected shock layer problem which is of primary interest is the end-wall radiative heat transfer time-history, i.e., the variation with time in the emitted radiative flux from the shock layer. These calculations are presented in Figures 4 and 6. Of particular interest is the relative importance of VUV radiation as compared to radiation in the visible and near infrared portions of the spectrum. As may be seen, at an initial driven tube pressure of 1.0 torr, Figure 4 indicates that for early times the

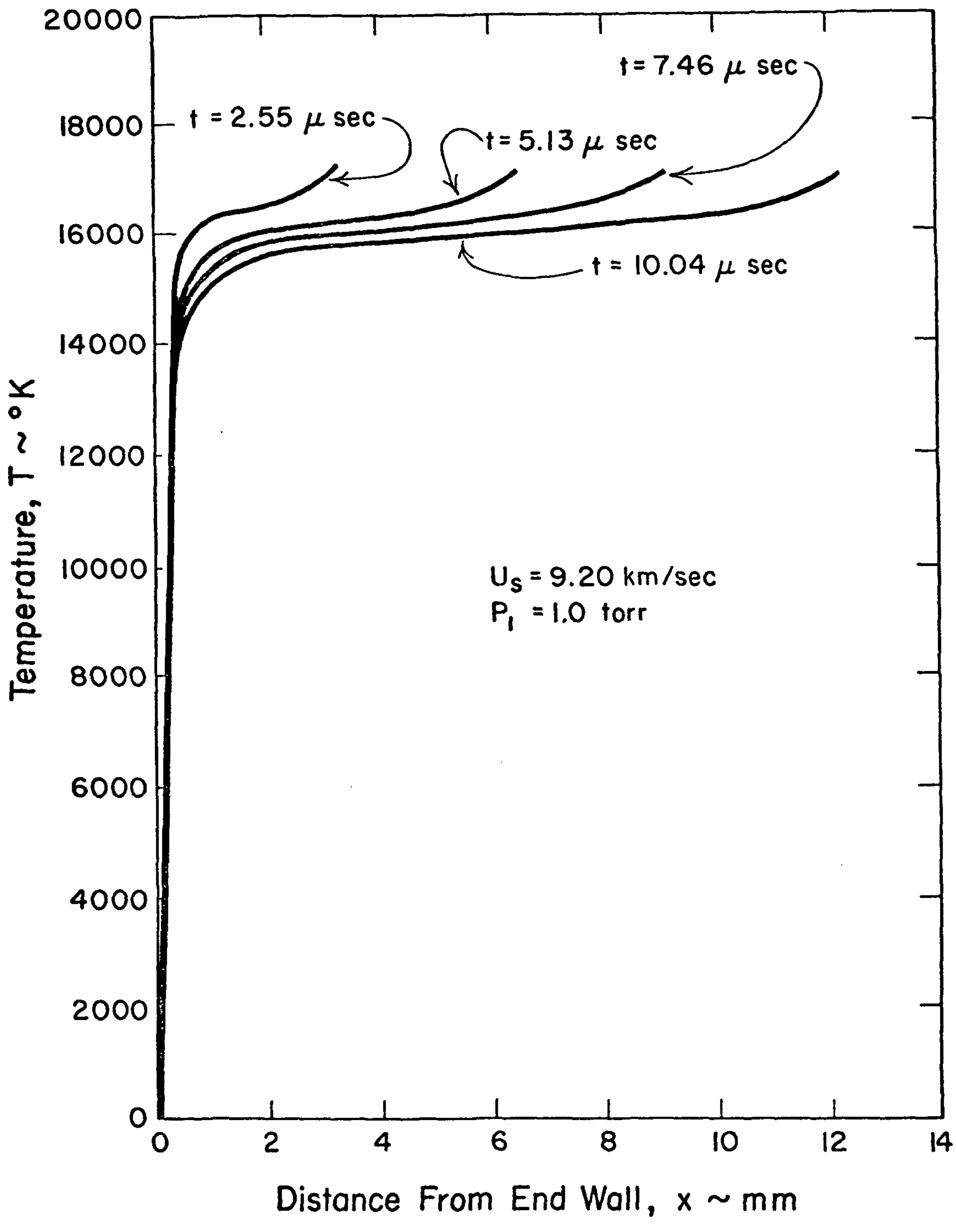

Figure 3 - Calculated Flow Field Temperature Distribution in Air for Different Times after Shock Reflection; U_s = 9.20 km/sec, P_1 = 1.0 Torr

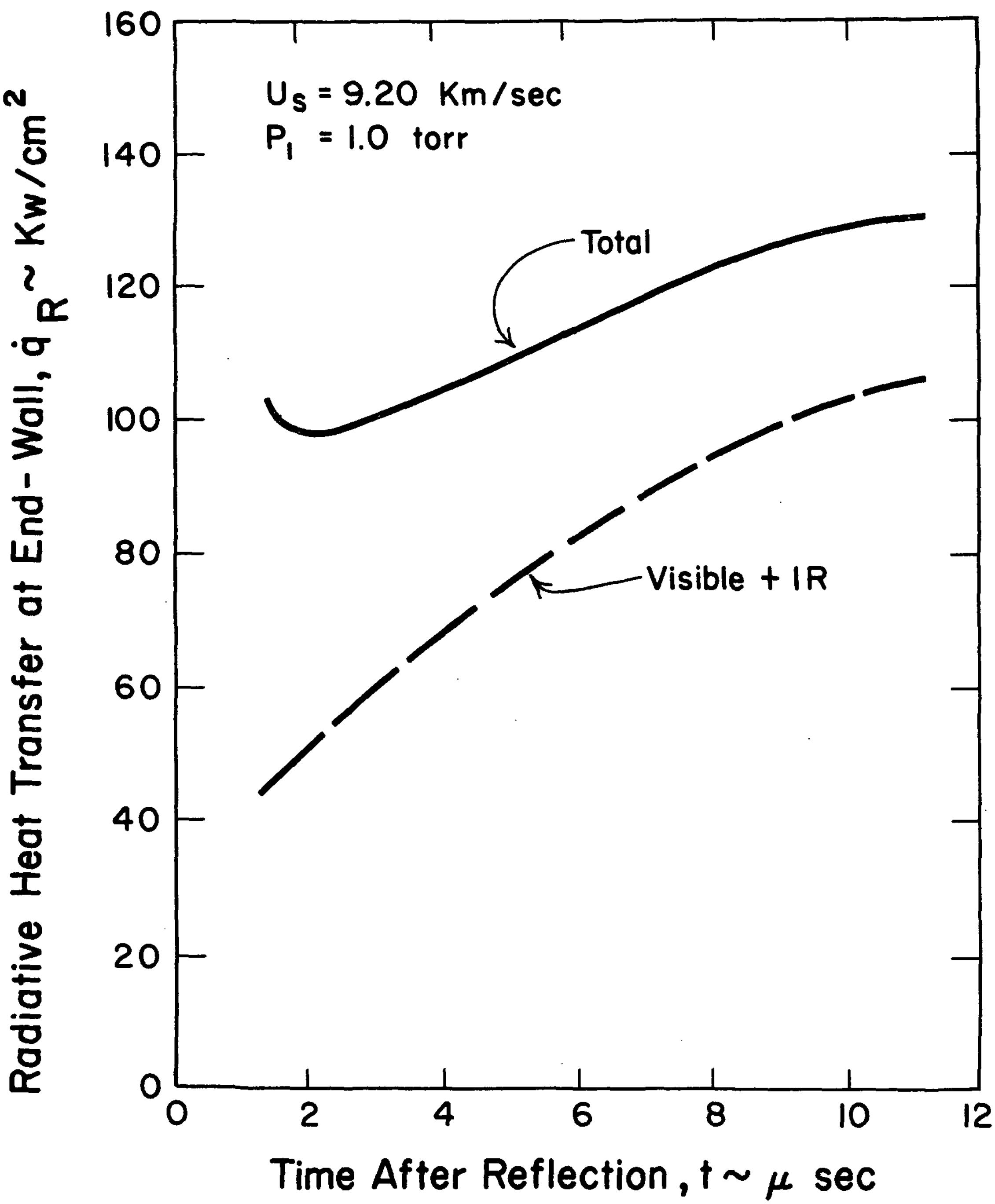

Figure 4 - End-Wall Radiative Heat Transfer Time-History in Air from Flow Field Calculations Using Five-Step Absorption Coefficient Model; U_s = 9.20 km/sec, P_1 = 1.0 Torr

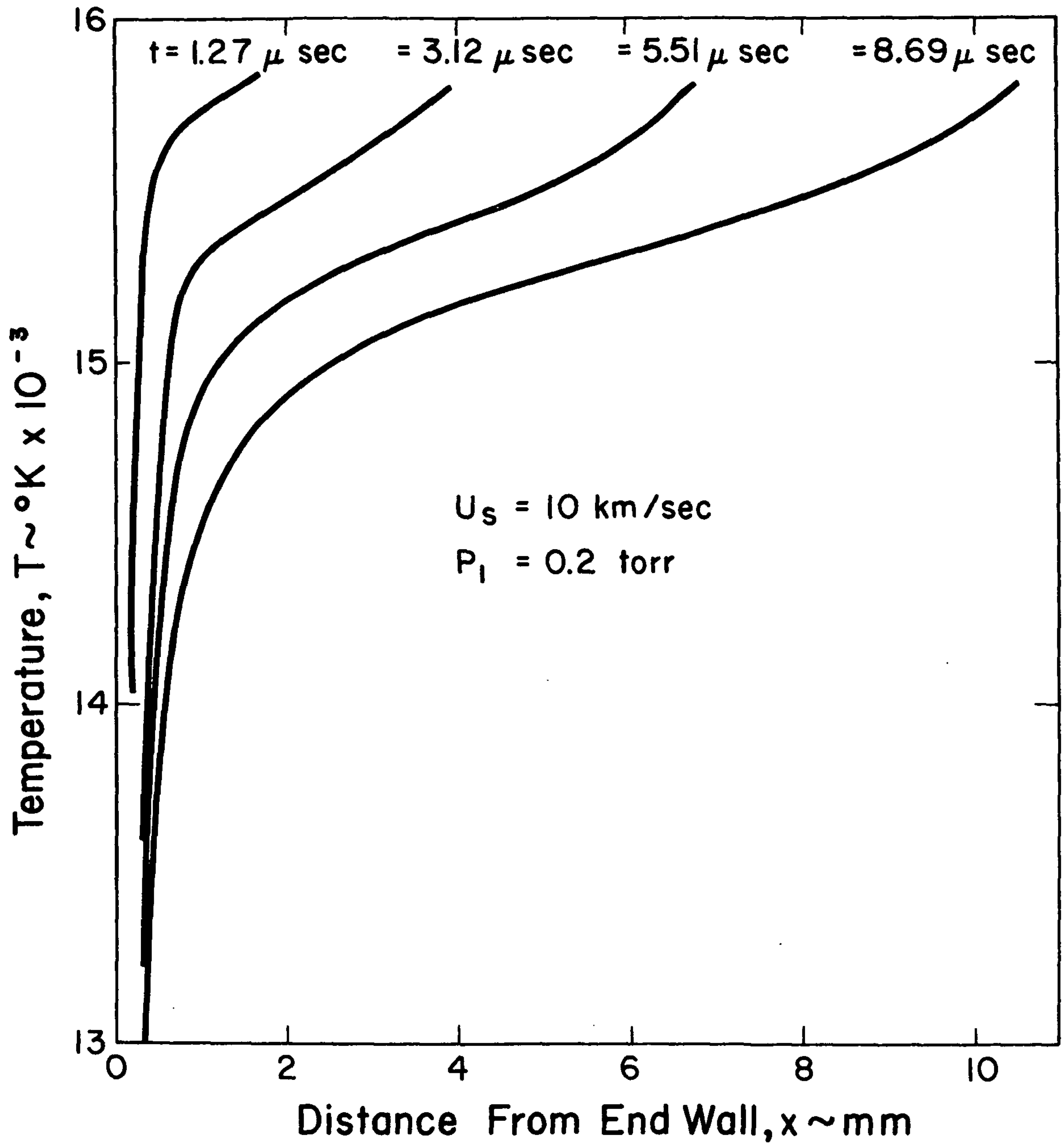

Figure 5 - Calculated Flow Field Temperature Distribution in Air for Different Times after Shock Reflection; U_s = 10 km/sec, P_1 = 0.2 Torr

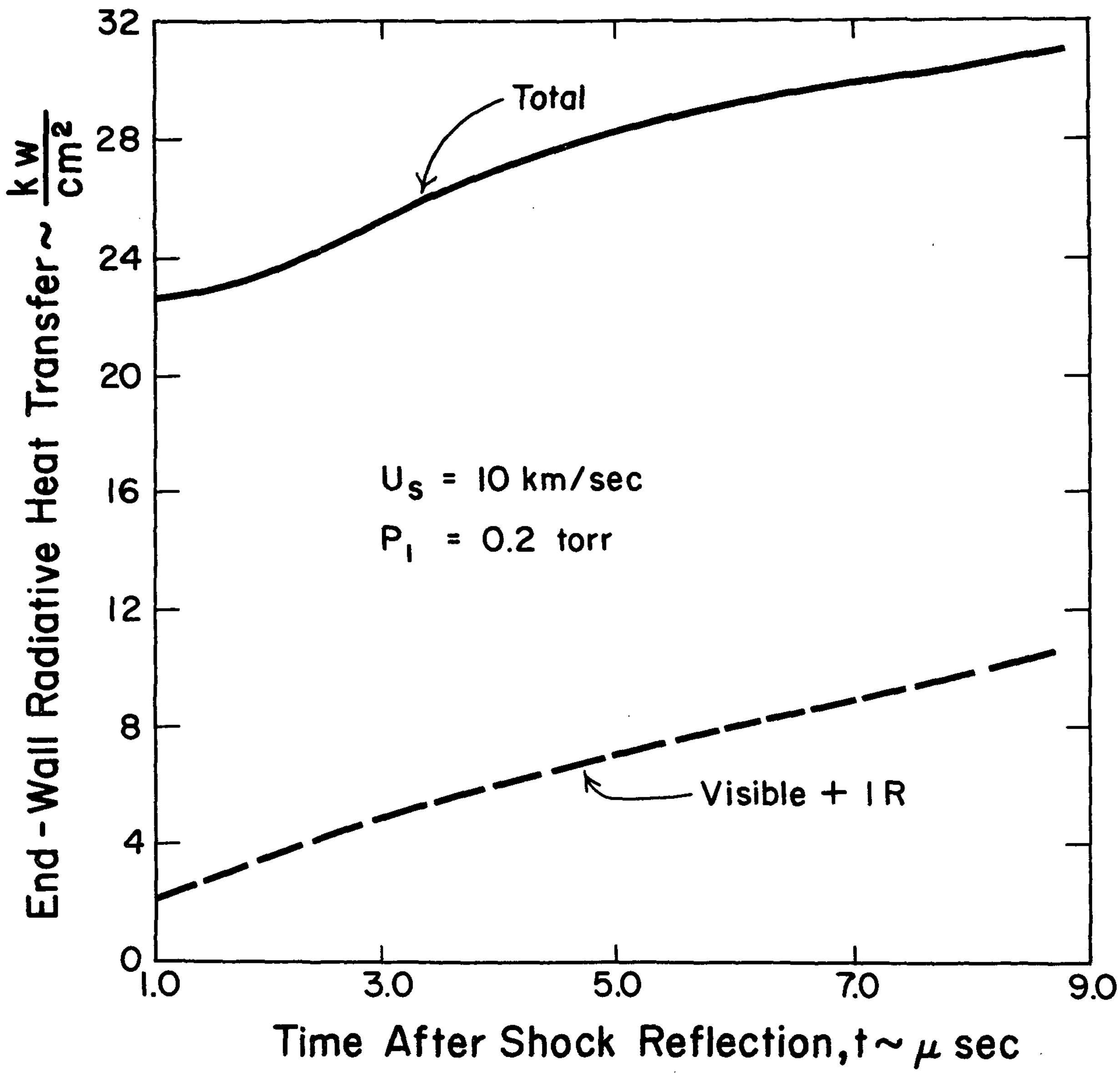

Figure 6 - End-Wall Radiative Heat Transfer Time-History in Air from Flow Field Calculations Using Five-Step Absorption Coefficient Model; U_s = 10 km/sec, P_1 = 0.2 Torr

VUV radiation makes an important contribution to the total end-wall heat transfer. However, at longer times on the order of 5 to 10 microseconds the visible and near infrared radiation clearly dominate the radiative energy loss. On the other hand, at the lower initial driven tube pressure case of 0.2 torr, it is the VUV radiation that dominates the end-wall heat transfer over the entire time period shown in Figure 6.

The calculated end-wall heat transfer time-histories shown in Figures 4 and 6 clearly reflect the combined influence of self-absorption and radiative cooling. Without these radiative transfer effects, the end-wall heat transfer would increase linearly with time as the reflected shock wave moves at a constant velocity away from the end-wall. For the conditions of Figure 4, the VUV is strongly self-absorbed and the VUV end-wall heat transfer rate can be seen to actually decrease as the gas near the wall cools. However, the visible and infrared radiation, though constantly increasing in magnitude, provides an end-wall heat transfer which also is influenced by absorption and cooling effects. For the conditions in Figure 6, the VUV radiation is still self-absorbed; however, the visible and infrared radiation is virtually transparent and any deviation from a linearly increasing end-wall heat transfer rate here is due to radiative cooling effects.

It should be noted that the radiative cooling not only influences the total end-wall radiative heat transfer, but also the end-wall conductive heat transfer. A similar solution (no radiation) for the end-wall thermal boundary layer results in a calculated end-wall conductive heat transfer of $70.8\ t^{-1/2}$ kW/cm^2 (where t is in μsec) for the conditions of Figures 3 and 4. However, from Figure 3, it can be seen that the enthalpy in the region of the thermal boundary layer edge has been reduced due to radiative cooling. At a time of approximately 10 microseconds after shock reflection, this reduction is on the order of 20 percent; and, thus, at this instant of time the actual end-wall heat flux due to conduction is approximately 18 kW/cm^2 (this may be compared with the results in Figure 4). This is actually an oversimplification of the end-wall boundary layer problem since in the presence of radiation the boundary layer must now match an inviscid, radiating flow with a finite gradient at its outer edge. However, the above explanation serves to demonstrate the importance of radiative coupling with the end-wall boundary layer and indicates that for these conditions the radiative heat transfer does in fact dominate at the end-wall for times greater than a few microseconds.

Another interesting aspect of the radiative cooling phenomena is the influence of radiation on the propagation of the reflected shock wave itself. Calculations are shown in Figure 7 for a range of incident shock velocities in air at an initial driven tube pressure of 1.0 torr. As may be seen, for the lower incident shock wave velocities, there is little shock attenuation. However, for the higher incident shock speeds, the attenuation due to radiative cooling is noticeable.

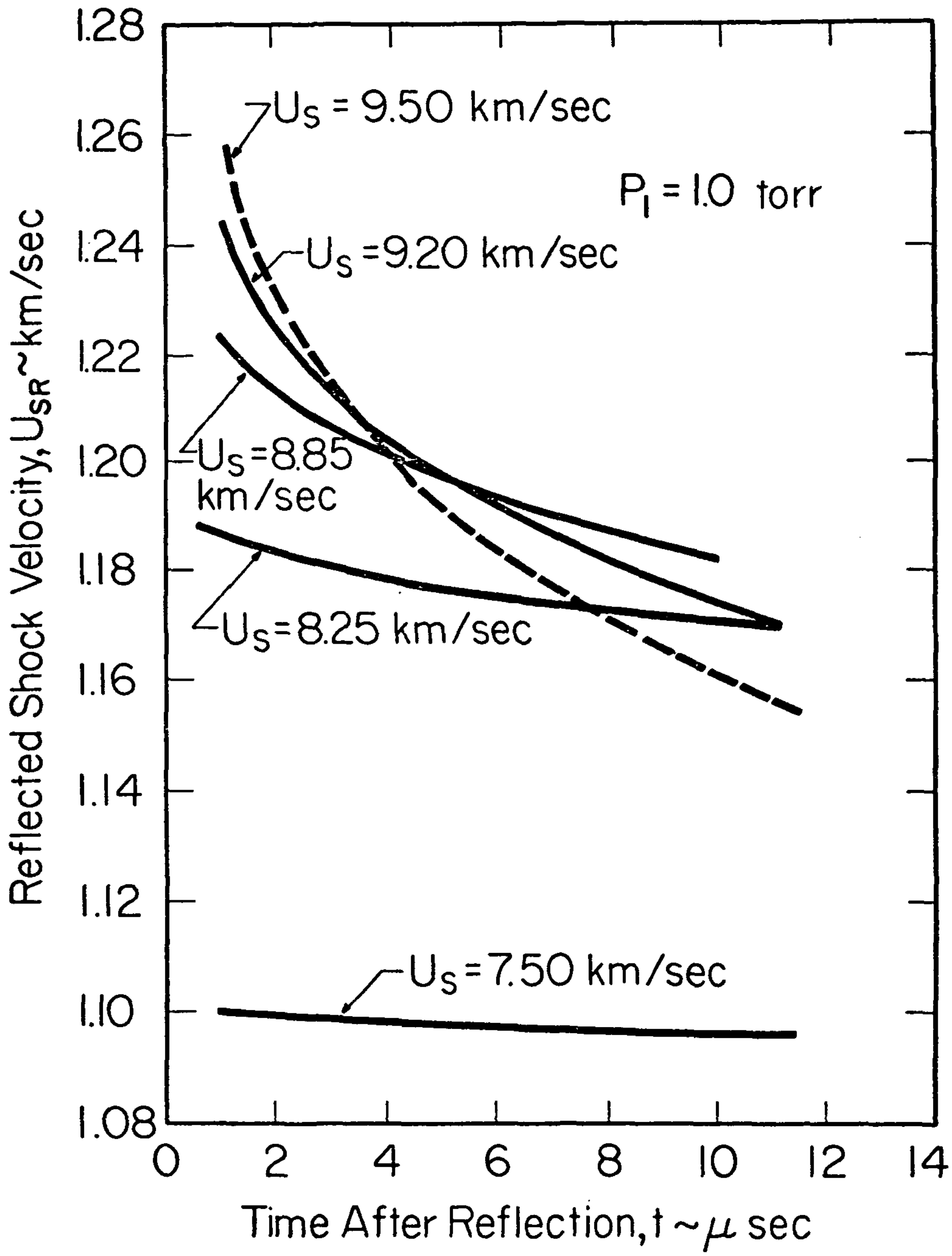

Figure 7 - Calculated Reflected Shock-Wave Velocity Time-History in Air

For example, for U_s = 9.20 km/sec, the shock velocity decreases by 5-10 percent over a 10 microsecond period; however, the conditions immediately behind the reflected shock wave remain virtually unchanged with time. This is illustrated by the results in Figure 3 and is due to the previously noted fact that the reflected shock strength is primarily governed by the conditions of the incident shock wave generated flow.

III. NONEQUILIBRIUM EFFECTS

At low initial driven tube pressures and/or for short times after shock reflection, important nonequilibrium effects may be present in the reflected shock wave processed gas. These nonequilibrium effects might include both ionization nonequilibrium and thermal nonequilibrium, e.g., an electron temperature different from the temperature of the heavier species present, and would manifest themselves through a coupling with each other and with the important radiative transport mechanisms which may be present. The result of a nonequilibrium coupling of the radiative transfer, ionization, and collisional processes would be not only altered shock layer properties, but also an alteration in the end-wall heat transfer and in the propagation of the reflected shock wave itself.

A major portion of the effort on this grant has been an investigation of such nonequilibrium effects. This has been carried out through numerical calculations of the post-reflected shock wave flow field including two temperature gas effects, i.e., separate electron and heavy body temperatures, finite rate ionization, and radiative emission and absorption. In the latter, the five-step model discussed briefly in the previous section was used and all calculations were carried out for nitrogen with both dissociation and ionization mechanisms being included. This analysis was carried out by Carlson and the details may be found in References 12-15. Although details of this analysis will not be repeated here, it is interesting to compare the characteristic times representative of the three basic processes of interest, i.e., radiative cooling, deionization, and thermal equilibration by collisions.

Such a comparison is shown in Figure 8 for two typical incident shock velocities and for a range of initial driven tube pressures. From Figure 8 it is apparent that the characteristic ionization recombination times at low pressures can be significantly longer than those required for radiative cooling. To increase the possibility of observing such a nonequilibrium radiative cooling effect, a reflected shock flowfield corresponding to an incident shock velocity of 11 km/sec and an initial pressure of 10^{-2} torr was selected by Carlson as the primary calculation condition. Admittedly, the reflected shock front is itself somewhat thick (relative to the shock layer thickness) for such a condition, but as can be seen in Figure 8, a lower initial pressure offers a greater probability of observing the coupling of radiative cooling and ionization relaxation. In addition, the 10^{-2} torr case represents an extreme in that if these results show

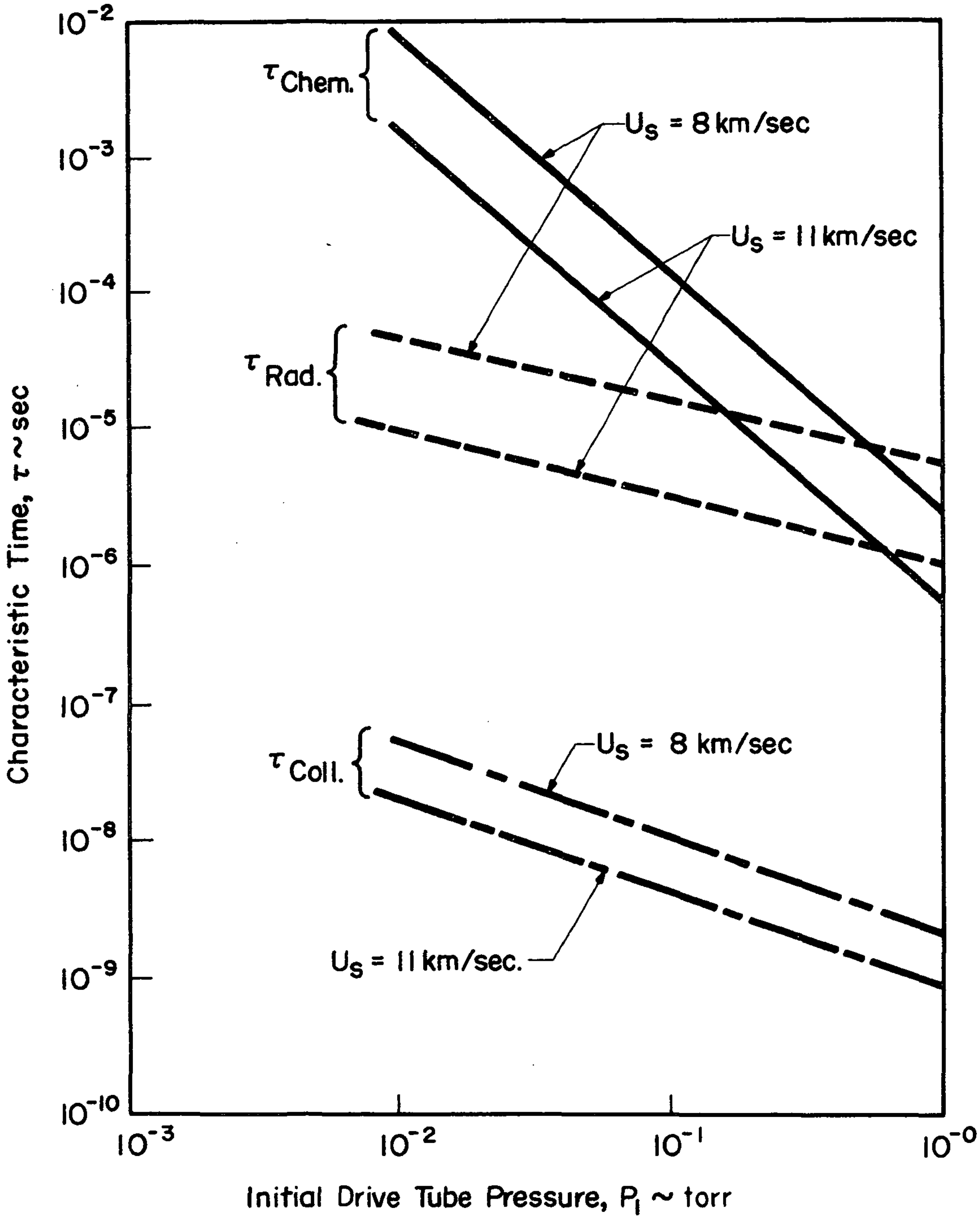

Figure 8 - Characteristic Times Behind Reflected Shock Waves in Nitrogen

no significant effects due to ionization and thermal nonequilibrium, then such effects can be assumed to be negligible at higher pressures where the shock front is, by comparison, thin.

The most significant of the results obtained by Carlson in these calculations is the prediction of strong radiative gasdynamic coupling at short times after shock reflection. Even though for these conditions the absorption coefficient in the vacuum ultraviolet is very large, the shock layer is so thin that the gas is essentially transparent and strongly radiating. Figures 9-12 show comparison calculations both with and without the inclusion of radiative cooling. Figure 9 compares the temperature profiles for the two cases for a time of 0.75 μsec after shock reflection. In the radiative cooling case, both the electron and heavy particle temperatures near the wall have values below 20,000°K; however, the non-cooled calculation exhibits heavy body temperatures greater than 25,000°K and electron temperatures around 22,000°K. In addition, the results for the radiatively cooled case indicate that at the wall thermal equilibration for all practical purposes exists for times longer than 0.45 μsec. However, in the non-radiative cooling case the wall heavy particle and electron temperatures are still over 4000°K apart at 0.75 μsec after shock reflection.

The shock position for the two calculations differs by about a factor of 2; this result is illustrated in Figure 10 where the reflected shock wave trajectory is shown on an x-t diagram. As is apparent, the reflected shock wave is predicted to come off the end wall at the frozen (no post-shock ionization or thermal equilibration) value of its velocity. For the first few tenths of a microsecond it propagates at that value before finally slowing down and asymptotically approaching the equilibrium reflected shock velocity at a time of about 1 microsecond after reflection. Because of its initial faster rate of propagation, at a time of 1 microsecond the reflected shock wave is considerably further from the end-wall than it would have been if it had been propagating at the equilibrium speed for its entire time history.

Further evidence of radiative transfer effects in the reflected shock layer appear in the velocity profiles shown in Figure 11. In the no-radiative cooling case, there is no evidence whatsoever of the strong velocity acceleration toward the wall that is so pravalent in the calculations including radiative cooling.

The variation in end-wall pressure is presented in Figure 12 and the result for the radiatively-cooled case here again reflects the effects of radiative transfer. From its initially relatively high value corresponding to frozen flow conditions, the end-wall pressure is seen to decrease to a minimum value at about 0.35 μsec after shock reflection, and then begins again to increase. At about 0.70 μsec it attains a value which remains relatively constant for the rest of the calculation and which is almost identical to the ideal equilibrium value of 3.6×10^5 dyne/cm^2. This rather marked initial decrease in

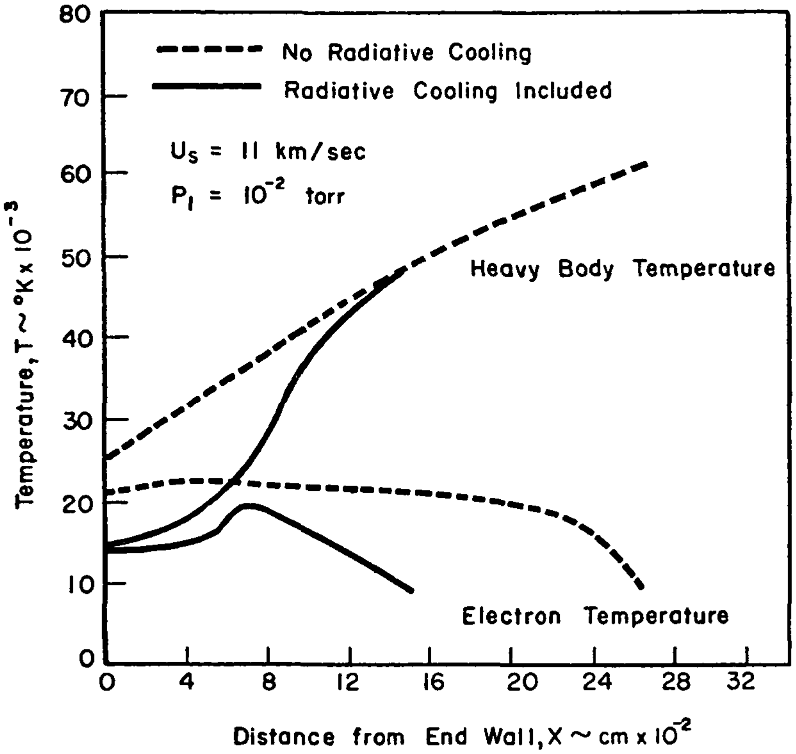

Figure 9 - Comparison of Electron and Heavy Body Temperature Profiles at 0.75 Microsecond after Shock Reflection with and Without Radiative Cooling

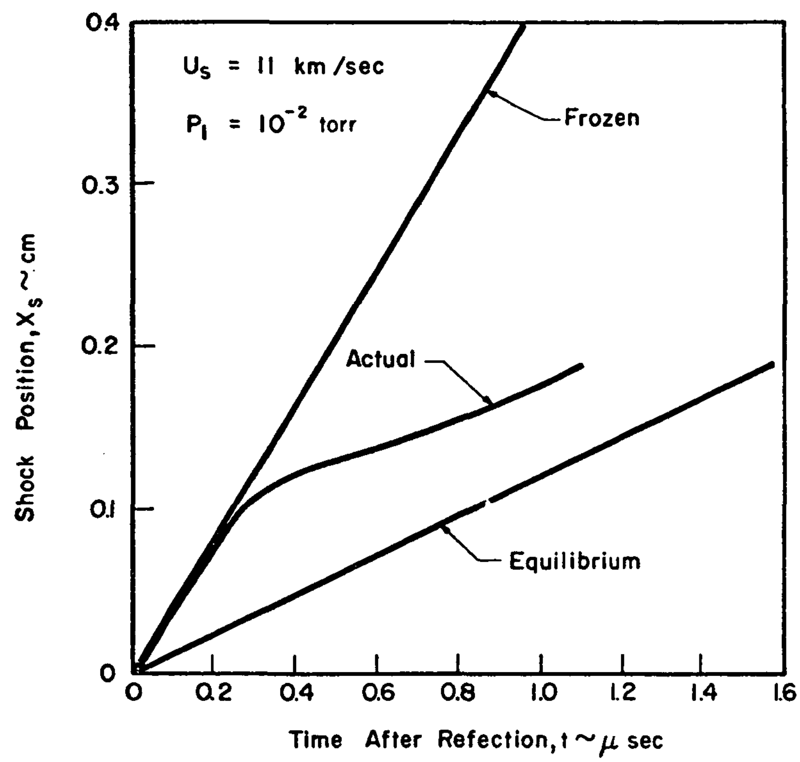

Figure 10 - X-t Diagram for Reflected Shock Wave in Nitrogen Illustrating Nonequilibrium Effect

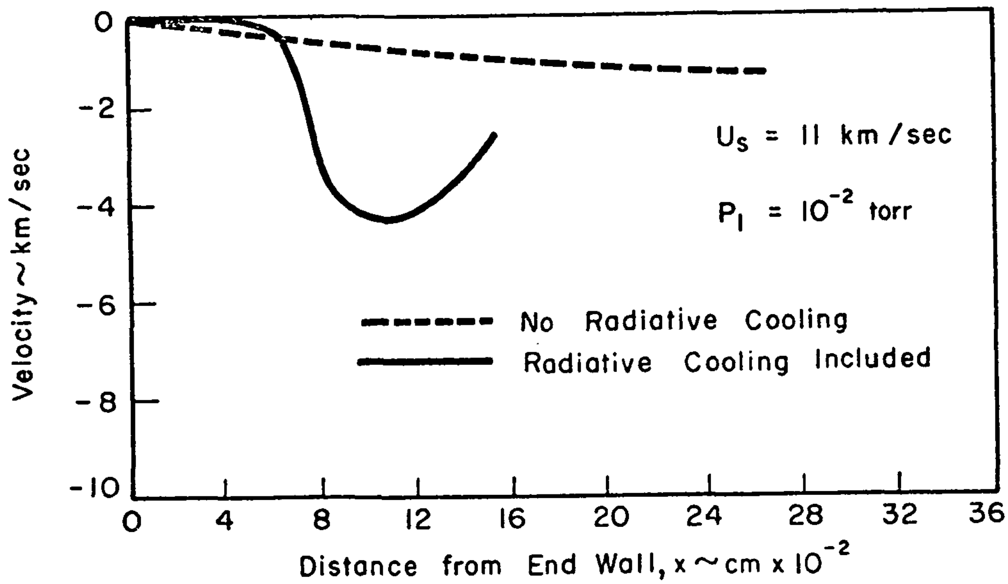

Figure 11 - Comparison of Velocity Profiles at 0.75 Microsecond after Shock Reflection With and Without Radiative Cooling

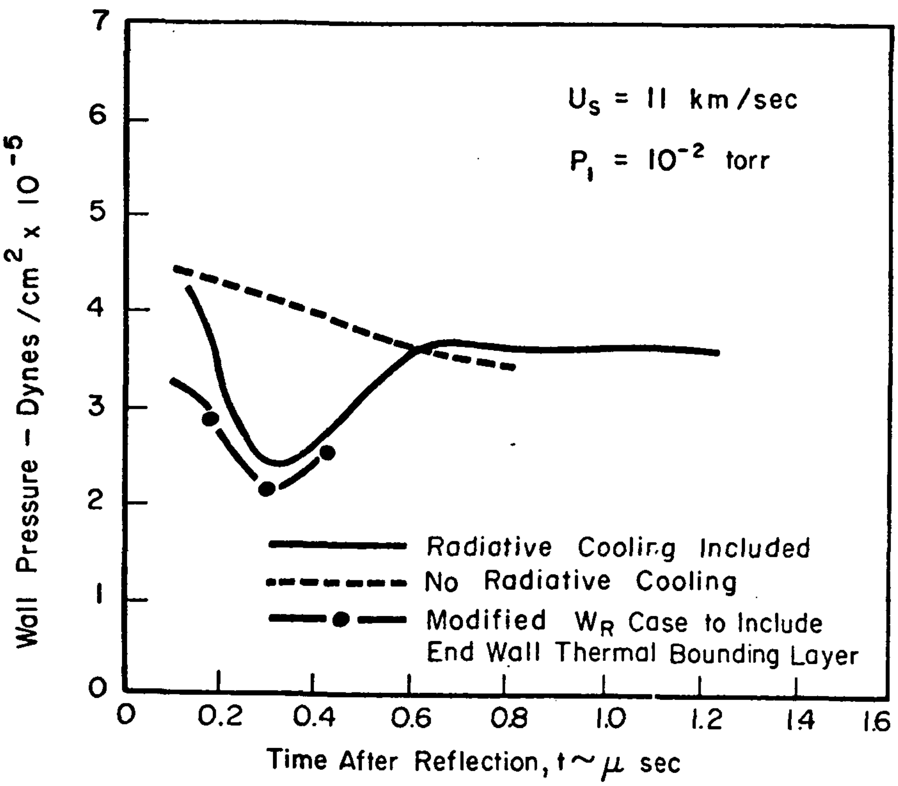

Figure 12 - Comparison of End-Wall Pressure Time-History With and Without Radiative Cooling

pressure of almost a factor of 2 is caused by the effects of radiative cooling, since in the non-cooled case the wall pressure is seen to decrease slowly and steadily from its frozen value to the equilibrium value without the dip evident in the complete calculation. As the gas cools due to radiation losses, the temperature drops precipitiously causing this dip in the calculation. However, the accompanying change in number density is small because no appreciable ionization has yet taken place and the pressure thus decreases.

To ascertain whether or not inclusion of end-wall thermal conduction, i.e., the end-wall thermal boundary layer, could affect these results, a calculation has been made with the initial reflected shock velocity equal to one-half the ideal frozen value. In this manner the maximum initial effect of thermal conduction on the inviscid flow is included.[16] The resulting end-wall pressure variation is also shown in Figure 12, and it is qualitatively identical to the radiatively cooled case. Thus, in comparison to radiative cooling, shock velocity variations resulting from thermal conduction have only a small effect on the end-wall pressure behavior.

Carlson investigated a number of other details with regard to the assumptions upon which his analysis was based but which are not discussed here; however, the end-wall heat transfer results obtained as part of these numerical flow field computations will be discussed in Section V.

IV. SHOCK TUBE EXPERIMENTS

The experimental measurements carried out as part of the effort on this grant were performed in The Ohio State University arc-driven shock-tube facilities. These shock-tube facilities included two separate shock tubes, each of which employed a 10-cm diameter driver section with coaxial electrodes recessed in a T-arrangement at the bottom of the driver as illustrated in Figure 13. The energy is supplied by a 200,000 joule, 6000-volt capacitor bank, and helium is used as the driver gas. The driven tube for these facilities is 9 m long and 10 cm in diameter. This tube may be either used with an end-plate, as, for example, in the study of reflected shock waves--in this case the vacuum system is connected through a 10-cm diameter valve which when closed preserves the contour of the shock tube--or with the driven tube terminated in a dump tank producing a high enthalpy, supersonic flow in the free-jet test region which may be used for aerodynamic studies. It is the former mode of operation which has been employed in obtaining the data presented here.

The incident shock velocity is measured using either ionization probes or photomultipliers to observe the passage of the shock wave at stations a known distance apart, while the initial driven tube pressure is measured using either a silicon fluid sloped U-tube manometer board or a McLeod gage. Maximum shock velocities on the order of 11 km/sec

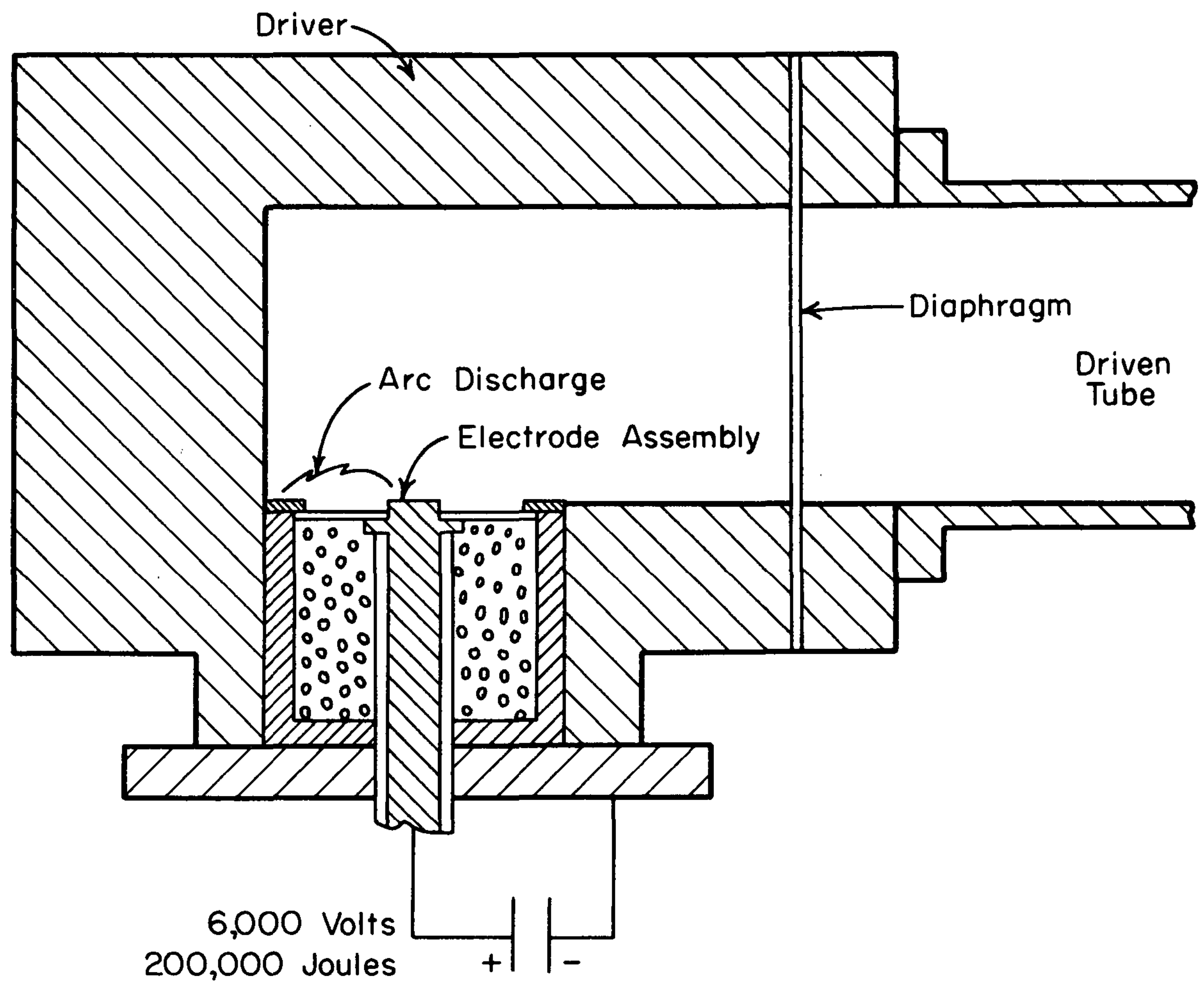

Figure 13 - Electrode System for the OSU Arc-Driven Shock Tube Facilities

and post-incident shock equilibrium temperatures in excess of 10,000°K in air and even higher in argon and other gases are attainable.

Shown in Figure 14 are the conditions attainable behind reflected shock waves in air. The indicated temperature and electron density are predicted post-reflected shock wave properties for equilibrium Rankine-Hugoniot conditions based on the reflection of an incident shock wave traveling at the velocity and in air at an initial pressure corresponding to the coordinates of the map. Also shown is the maximum attainable velocity in the OSU arc-driven shock-tube facilities as a function of initial pressure; it can be seen that temperatures in excess of 15,000°K and electron densities on the order of 10^{18} particles/cm^3 are attainable.

It should be noted that the unique driver design, using coaxial electrodes recessed in a T-arrangement, minimizes driver gas contamination and radiation. This is obviously of importance in high temperature experimental studies, particularly in studies of reflected shock wave radiation. Furthermore, the arc is extinguished considerably before diaphragm rupture and, thus, there is no influence of the arc discharge process on the nature of the shock tube phenomena observed.

These facilities have been used extensively in earlier experimental investigations;[17-18] and the flow conditions, including the available test duration, have been previously investigated. The test time for the reflected shock studies in air is on the order of 10-15 microseconds.

The objectives of the particular experiments carried out as part of this effort were as follows:

(1) To obtain an indication of the nature of the reflected shock flow field;

(2) To obtain verification of the one-dimensionality of the reflected shock wave;

(3) To obtain measurements of the total conductive and radiative end-wall heat transfer and of the end-wall radiative heat transfer itself;

(4) To obtain measurements of the reflected shock wave velocity time-history.

All experiments were carried out using air as the test gas, and the effort in each of these areas is summarized (the numbering of these areas of activity below corresponds to the numbers used above).

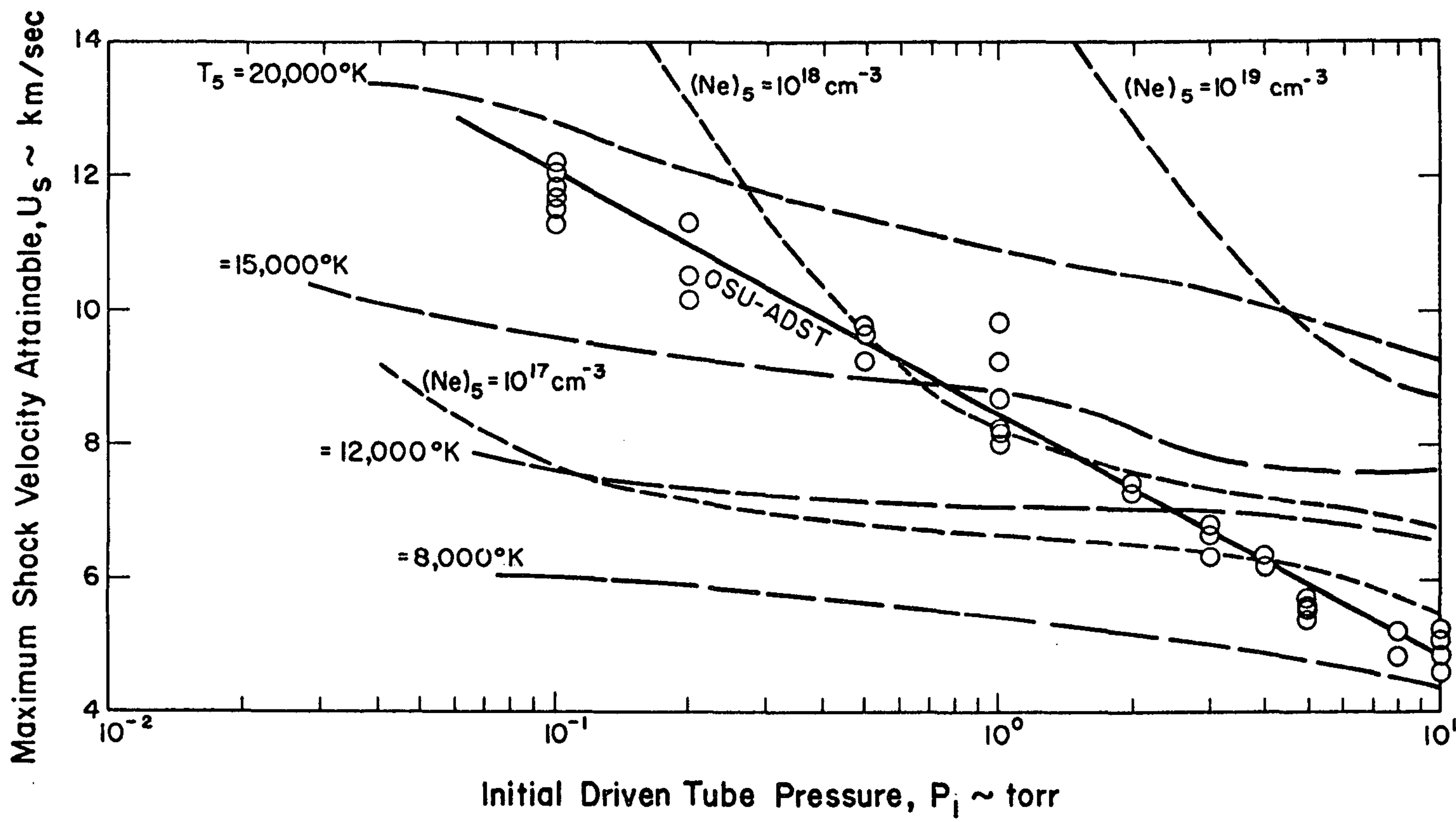

Figure 14 - Post-Reflected Shock Wave Conditions in Air Attainable in Ohio State University Arc-Driven Shock Tube Facility

1. Broad-Band Photomultiplier Radiative
Intensity Measurements

Broad-band photomultiplier measurements of the radiation time-history behind reflected shock waves in air were carried out with the 1P22 photomultiplier tubes looking across the tube through a collimated slit system mounted on the side-wall.[4] In Figure 15 a selected photomultiplier measurement of the gas radiative intensity is shown, and significant radiative cooling is indicated.* Although this measurement is for an incident shock wave velocity of 9.50 km/sec, similar measurements have indicated noticeable cooling at shock velocities below 9 km/sec for an initial pressure of 1.0 torr.

As may be seen in Figure 15, approximately 3 microseconds prior to the arrival of the reflected shock wave at the slit position, the measured radiation begins to increase. The slit is located 0.4 cm from the end-wall; based on the calculated reflected shock wave velocity, the beginning of this increase corresponds to the moment of shock wave reflection. This increase in intensity is radiation emitted from the reflected shock region and reflected from the shock tube wall. As the reflected shock wave moves away from the end-wall and towards the slit, the reflected radiation increases, and with the arrival of the reflected shock wave, the photomultiplier output sharply increases, peaks, and then begins to decay as cooling sets in.

2. Luminosity Photographs of Reflected
Shock Wave Front

Luminosity pictures of reflected shock waves in air have been obtained using a 50-nanosecond exposure Kerr Cell Shutter[19,20]; these photographs tend to verify the planar nature of the reflected shock wave. Although only a limited number of pictures have been obtained, they do demonstrate that the reflected shock wave is planar everywhere, with the only exception being near the side-wall. Figure 16 is a luminosity photograph for an incident shock velocity of 9 km/sec in air at an initial driven tube pressure of 1.0 torr. The end wall is to the right, and although some shock curvature is observed to occur, the reflected wave does appear to be planar in the center region of the tube. One of the major emphases of this overall effort has been to obtain measurements of end-wall heat transfer. These measurements have been carried out in the center of the end wall. Based on the luminosity photographs, it appears that this region should be approximately one-dimensional and, thus, the use of the one-dimensional assumption in the analysis of the end-wall heat-transfer data should be justified.

*More quantitative measurements are now being carried out on NASA Grant NGL-36-008-163.

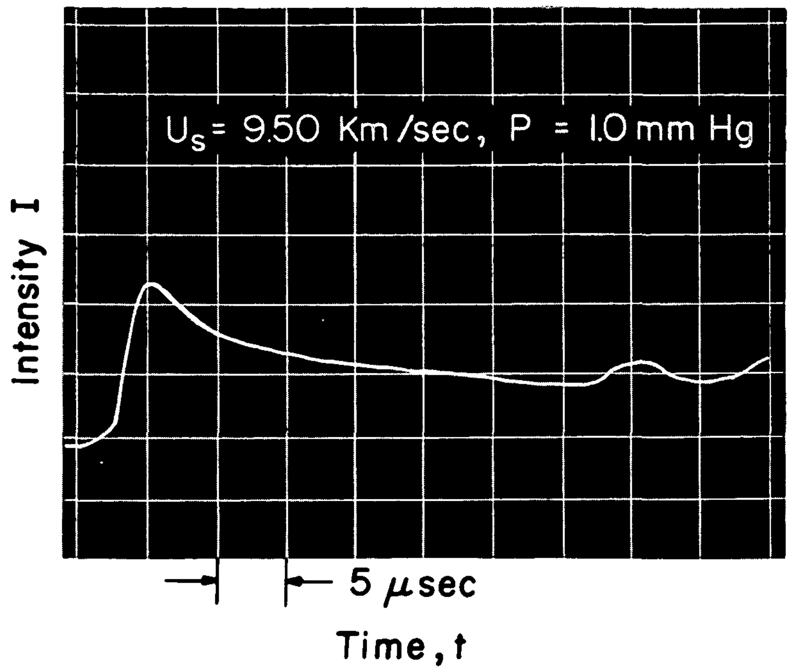

Figure 15 - Photomultiplier Measurement of Radiative Time-History Behind Reflected Shock Wave in Air

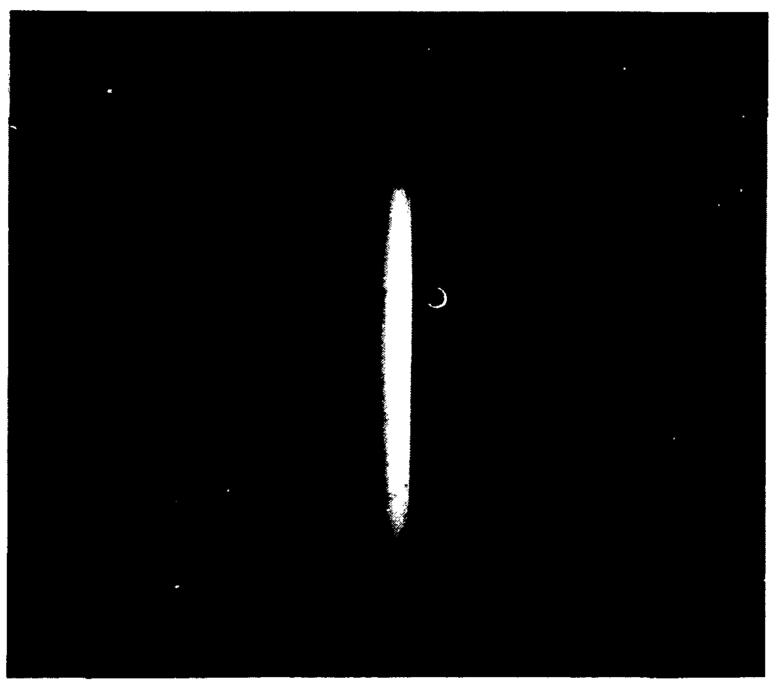

Figure 16 - Luminosity Photograph of Reflected Shock Wave in Air, U_s = 9 km/sec, P_1 = 1.0 Torr (end-wall to the right)

3. End-Wall Heat Transfer Measurements

End-wall radiative heat transfer measurements have been carried out in air at an initial driven tube pressure of 0.1 torr. These measurements were performed using a thin film gage mounted behind a sapphire window and observed the wavelength region of 0.17 to 6 microns. They are an extension of earlier measurements carried out at an initial pressure of 1.0 torr.[22] The data obtained as a part of this series of measurements are shown in Figure 17 where the end-wall radiative heat transfer rate at a time of 6 microseconds after shock reflection is shown as a function of incident shock velocity. These radiative heat transfer measurements are time-resolved and provide a measurement of the end-wall heat flux as a function of time over the entire test period. It is only for the sake of convenience and brevity that the comparisons shown here are limited to a single specific time after shock reflection.

Also shown in Figure 17 are two separate theoretical calculations. The one calculation is for a transparent homogeneous slab, i.e., zero radiation loss, transparent gas; the other is also for a homogeneous slab, but includes self-absorption using the five-step absorption coefficient model discussed in Section II. Neither of these two calculations include radiative cooling, and both calculations are based on equilibrium post-reflected shock conditions. The data appears to favor the transparent gas calculation, being if anything, slightly higher. However, these data are perhaps misleading since a look at Figure 8 suggests that the assumption of equilibrium may not be valid.

As will be discussed in the next section, the effect of non-equilibrium appears to enhance radiative emission. As will also be seen in the next section, the previously obtained data at a pressure of 1.0 torr[22] indicates a lower end-wall radiative heat transfer than that predicted by either type of calculations shown in Figure 17. Thus, there is a distinct difference in the interpretation of these two sets of data.

In addition to these measurements of end-wall radiative heat transfer, the measurement of the total end-wall heat transfer including both vacuum ultraviolet radiation and thermal conduction was considered to be of high priority as part of this effort. A number of possible measurement techniques were considered for this application. One such possibility is the use of a calorimeter type gage [23] which lends itself readily to the measurement of constant heating rates. As may be seen by taking the total radiative heat transfer from Figure 4 and adding to this the end-wall conductive heat transfer, the total end-wall heat transfer rate is approximately constant during a time interval of 1-10 microseconds after shock reflection. Following Reference 23, calculations of the second order correction to the resistance change of a platinum calorimeter gage have been carried out for total heat-transfer rate time-histories approximately equal to that for typical reflected shock conditions such as those in Figures 4 and 6.

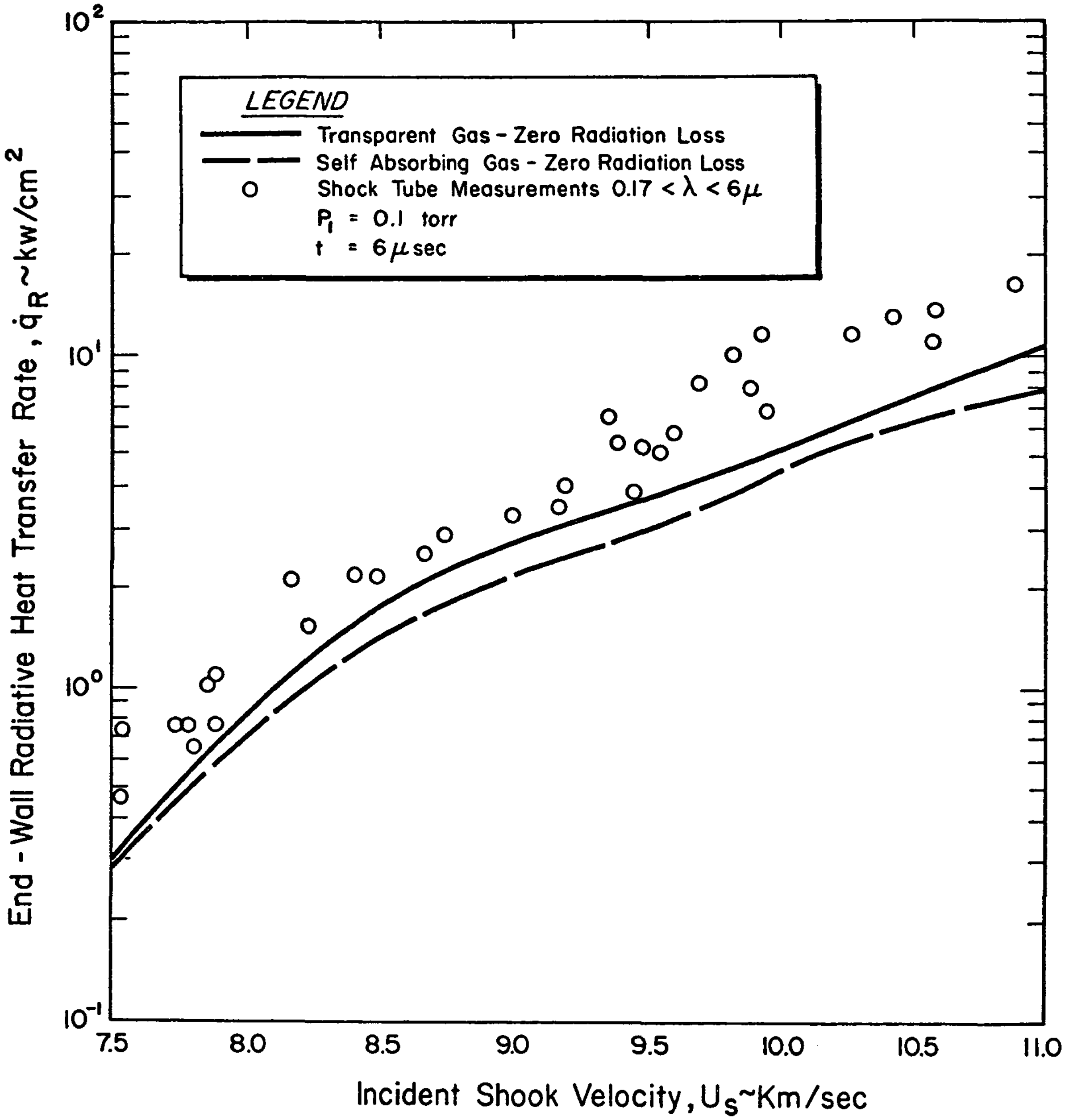

Figure 17 - End-Wall Radiative Heat Transfer Measurements in Air

These results indicate that in using the time derivative of the output of a calorimeter gage to determine the instantaneous heating rate an error of as much as 20 percent would be encountered.

Although these results are not particularly encouraging, a few preliminary data points were obtained using a platinum calorimeter gage coated with a thin film of Luster Black No. 4771 (this coating is also used on the radiative heat transfer gages[21]). As an example, for an incident shock velocity of 8 km/sec and a pressure of 1.0 torr, a heating rate of approximately 60 kW/cm^2 was measured in this manner. Based on calculations, at t = 10 microseconds after shock reflection the radiative heat transfer rate will be at the most 40 kW/cm^2 including radiative cooling effects, while the conductive heat transfer rate is approximately 15 kW/cm^2. This makes a total heating rate for this condition of 55 kW/cm^2 which is in reasonable agreement with the measurement.

Only a limited amount of data were obtained in this manner, and because the magnitude of the second order correction is a complicating factor in any data interpretation, it was decided not to continue the development of this particular application of the calorimeter gage technique. Other techniques were considered, e.g., the use of an infrared bolometer;[24] however, no techniques have proved to be satisfactory.

4. Reflected Shock Wave Velocity Time History Measurements

Measurements of the reflected shock wave velocity time history for strong incident shock waves in air have been carried out using a rotating drum camera to monitor the reflected shock front radiation emitted from a horizontal slit in the shock tube wall.[22] Kodak Plus-X film was used; this system, with a slit height of 50 microns, gives a time resolution of 0.1 microsecond. These measurements are important because the reflected shock wave velocity will vary significantly with radiative cooling.

The data obtained, in general, show that with increasing incident shock velocity the attenuation of the reflected shock wave with time becomes more severe. This is expected if the effect is due to radiative cooling. Apparently this is the case since the measurements are in reasonable agreement with previous numerical calculations of this effect which will be discussed in the following section.

Selected reflected shock wave velocity time-histories obtained from these measurements are reproduced in Figure 18. The data also show that the reflected shock wave begins to accelerate approximately 4 or 5 microseconds after reflection from the end wall. This acceleration is consistently present in all the measurements with the beginning of the acceleration coming increasingly later with increasing incident shock velocity.

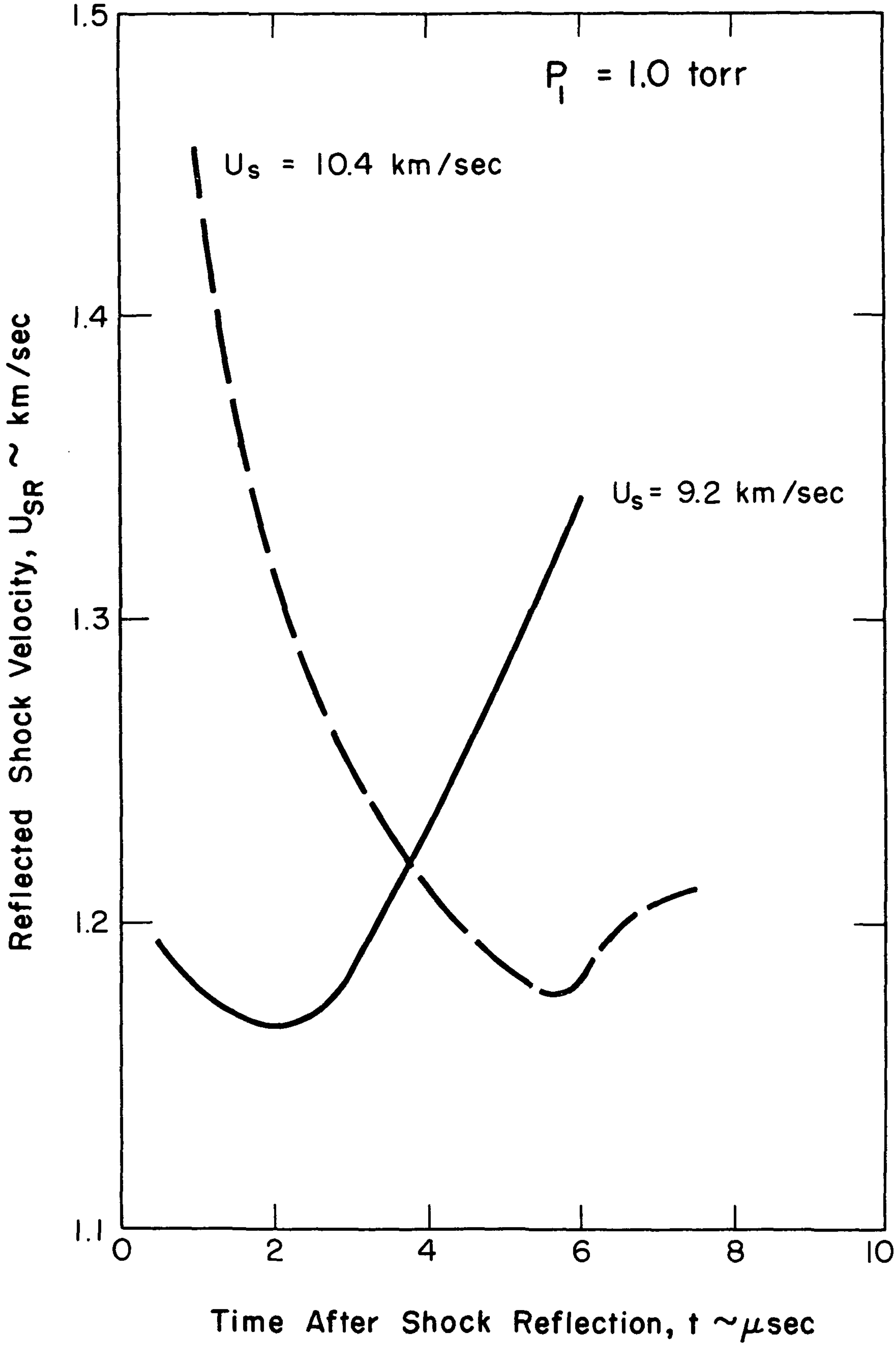

Figure 18 - Measured Reflected Shock Wave Velocity Time-Histories in Air

Considerable thought has been given to what could cause this acceleration and the possibilities include interaction with the side wall boundary layer, interaction with the contact region, and effects due to the expansion wave (produced at the diaphragm) catching up and interacting with the reflected shock wave. Of these possibilities, the most logical explanation appears to be that the reflected shock wave interacts with the sidewall boundary layer and as a result is accelerated. This effect by itself has been noted in previous shock tube studies.[26,27]

V. CONCLUDING DISCUSSION

Some summarizing comments will be offered based on comparisons between the theoretical calculations carried out and the experimental data obtained.

1. With regard to end-wall radiative heat transfer it appears that barring nonequilibrium effects, reasonable predictions can be made with relatively simple absorption coefficient models. This is demonstrated by the comparison shown in Figure 19 between the measured end-wall heat transfer rates of Reference 22 and numerical calculations, including both self-absorption and radiative cooling using the five-step model discussed in Section II.

It is of interest to consider the importance of the absorption coefficient model in somewhat more detail. This is shown in Table 2 for reflected shock conditions corresponding to an incident shock wave velocity of 8.85 km/sec in air at an initial pressure of 1.0 torr. Presented there is the above noted calculation, as well as those for (1) a transparent gas, (2) an isothermal slab with a non-gray gas whose absorption properties are based on the five-step model, (3) a gray gas, and (4) a non-gray two-step model based on the same radiative properties as previously discussed. These calculations are for a time of ten microseconds after shock reflection, with the mean of the corresponding data being 65.2 kW/cm^2. Table 2 shows that the transparent gas, the gray gas, the non-gray gas without radiative cooling, and the two-step non-gray models, when used in the indicated flow field calculations, all give results which are considerably high. Only the five-step model in a calculation including radiative cooling gives reasonable agreement with the mean of the data.

2. With regard to the observed attenuation of the reflected shock wave as it moves away from the end wall, this also has been found to be in agreement with numerical calculations of the type discussed in Section II. Results are shown in Figure 20 where the measured and predicted reflected shock wave deceleration rate are presented for a time of 1 microsecond after shock reflection. Although the overlap between the calculations and the data is somewhat limited, the agreement is reasonable and the trend is consistent.

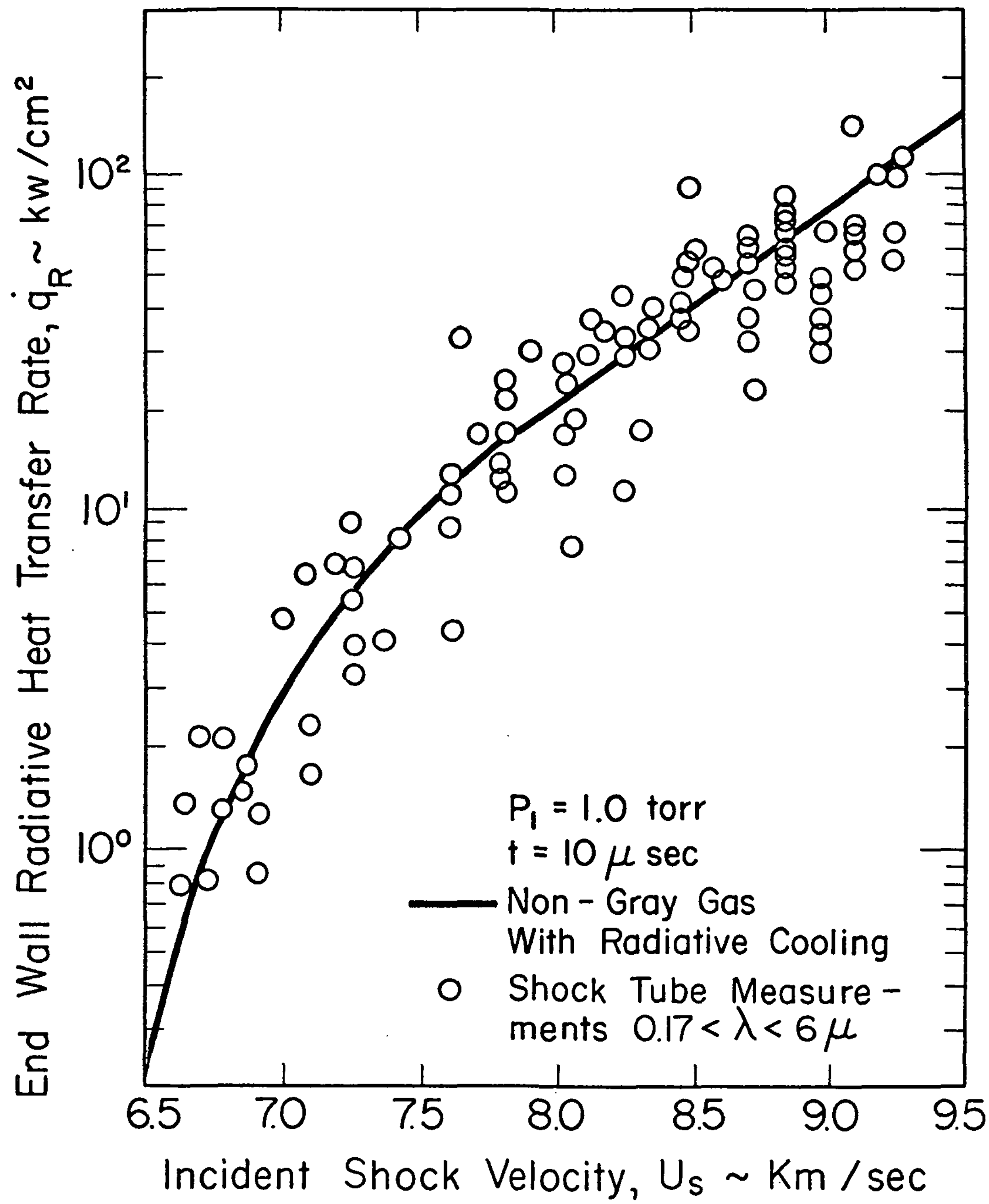

Figure 19 - Comparison of Shock-Tube End-Wall Radiative Heat Transfer Measurements with Theoretical Calculations for a Time of 10 Microseconds after Shock Wave Reflection

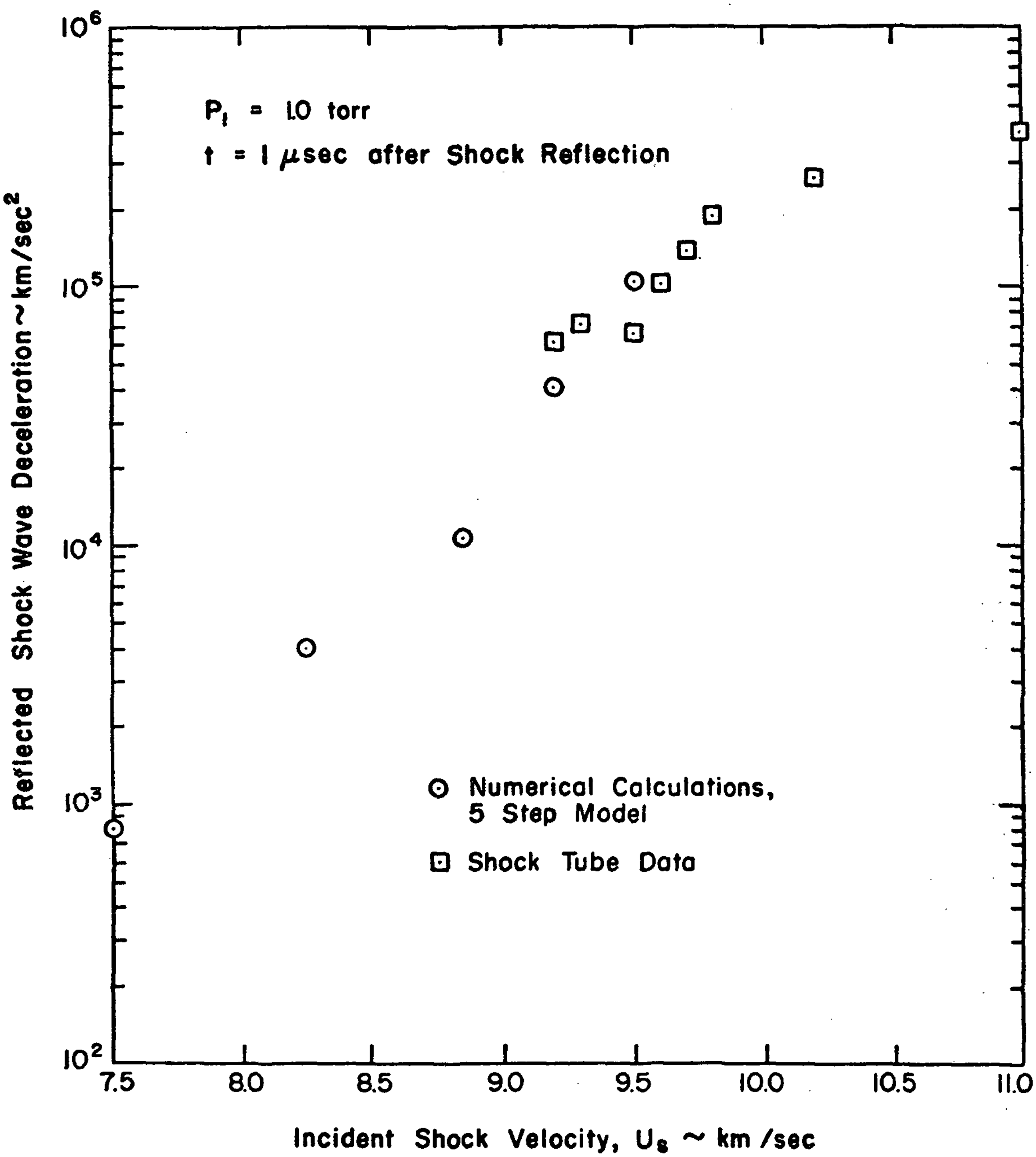

Figure 20 - Comparison of Predicted and Measured Reflected Shock Wave Attenuation Rates in Air

Table 2. Calculated End-Wall Radiative Heat Transfer (U_s = 8.85 km/sec, P_1 = 1.0 torr, t = 10 μsec)

Radiation Model	Vacuum Ultraviolet Heat Transfer, kW/cm^2	Visible Near Infrared Heat Transfer, kW/cm^2	Total Heat Transfer, kW/cm^2
Transparent Gas, no Radiative Cooling	1.93×10^4	247	1.95×10^4
Non-Gray Absorption (5-Step Model), no Radiative Cooling	70.3	115	185
Gray Gas Absorption With Radiative Cooling	6.47	102	108
Non-Gray Absorption (2-Step Model) With Radiative Cooling	1.71	97.3	99.0
Non-Gray Absorption (5-Step Model) with Radiative Cooling	12.1	61.7	83.8
Mean of Shock Tube Data	---	65.2	---

Obviously, the subsequent acceleration of the reflected shock wave is somewhat perplexing, although as noted earlier, such a phenomena has been noted in previous shock tube studies at lower shock velocities. Since the strength of the reflected shock wave is virtually entirely controlled by the conditions of the post-incident shock flow, it is felt that this acceleration has little effect on comparisons of the type shown in Figures 19 and 20.

3. Although part of a separate effort, recent measurements of the brightness temperature time-history behind reflected shock waves in air at an initial driven tube pressure of 1.0 torr indicates good agreement with calculations of the type discussed in Section II and presented in Figures 3 and 5.

Consequently, the effects of radiative cooling and self-absorption are not only important behind reflected shock waves in air at conditions attainable in arc-driven shock tubes, but these effects can be taken into account in numerical flow field calculations using a relatively simple absorption coefficient model of what must be considered as rather complex spectral characteristics. This, of course, must be qualified by the statement that no ablation phenomena is present in either the calculations or the experiments, and with ablation, more complex absorption coefficient models may be necessary.

An absorption coefficient model similar to the present five-step model has been used by Page et al. in carrying out theoretical calculations of stagnation point radiative heat transfer at hypervelocities.[28] Because of the similarities between the absorption coefficient models, the present agreement with experiment indirectly supports the results of Page et al., and it is felt that such absorption models should prove useful in future studies of radiative gasdynamics.

4. Turning to the influence of nonequilibrium phenomena in the reflected shock wave problem, the most unexpected result of the analysis carried out as part of this effort was the pressure dip illustrated by the results in Figure 12. In order to determine at least approximately the effect of incident shock velocity and initial pressure on this result, Carlson carried out two additional calculations corresponding to incident shock waves at velocities of 8 km/sec and 11 km/sec, respectively, in nitrogen at an initial pressure of 0.1 torr. Figure 21 compares the end-wall pressure variation for these two cases with that of Figure 12, and it can be seen that the pressure decrease due to radiative cooling also occurs at this higher pressure for the 11 km/sec case. However, at the 8 km/sec condition there is no evidence of the radiative cooling induced pressure dip. Since radiative effects are strongly dependent upon temperature and thus on shock velocity, this result is not too surprising, but it does serve to indicate that the magnitude of the radiation is a primary factor in determing whether or not the type of radiative transfer effect on end-wall pressure depicted in Figure 12 will occur.

5. There is evidence from the calculations carried out that the influence of nonequilibrium is to greatly enhance the magnitude of the end-wall radiative heat transfer as illustrated in Table 3, where the total end-wall radiative heat flux at a time of approximately 1 microsecond after shock reflection is shown for a variety of initial driven tube pressures and incident shock velocities; this was also suggested by the data obtained at 0.1 torr and the comparisons with theory shown in Figure 17. This nonequilibrium enhancement may be of engineering significance, e.g., in the thermal load encountered by space vehicles during the early stages of planetary atmosphere entry.

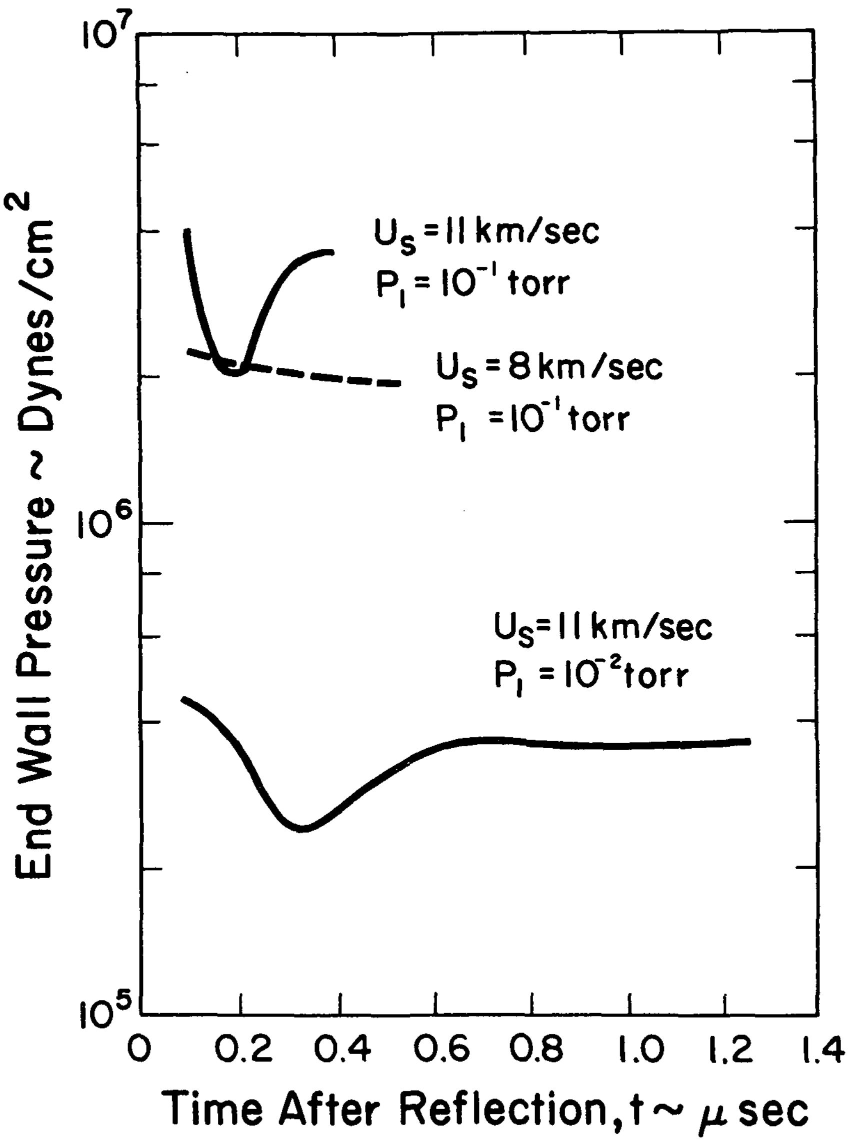

Figure 21 - Comparison of End-Wall Pressure Time-Histories for Selected Reflected Shock Wave Conditions

Table 3. Calculated Total End-Wall Radiative Heat Transfer at Short Times After Shock Reflection

Incident Shock Velocity U_s, km/sec	Initial Pressure P_1, torr	State of Gas	Time After Shock Reflection, t, μsec	Total End-Wall Radiative Heat Transfer, q_R, kW/cm^2
11	0.01	Nonequilibrium	1.0	6.4
8	0.1	Nonequilibrium	0.5	8.5
11	0.1	Nonequilibrium	0.6	110
8	0.2	Equilibrium	1.0	3.05
10	0.2	Equilibrium	1.0	23.2
8.25	1.0	Equilibrium	1.0	30.0
9.5	1.0	Equilibrium	1.0	165

REFERENCES

1. Laird, J. D. and Heron, K., "Shock Tube Gasdynamic Charts. Part I: Equilibrium Argon-Free Air from 3,000 to 40,000°K, Avco-RAD TM 64-12, April 10, 1964.

2. Allen, R. A., Rose, P. H., and Camm, J. C., "Nonequilibrium and Equilibrium Radiation at Super-Satellite Re-entry Velocities," Avco-Everett Research Laboratory Report RR 156, 1962.

3. Nerem, R. M., Carlson, L. A., and Hartsel, J. E., "Chemical Relaxation Phenomena Behind Normal Shock Waves in a Dissociated Freestream," AIAA Journal, Vol. 5, No. 5, May 1967, 910-916.

4. Nerem, R. M., Carlson, L. A., and Golobic, R. A., "Radiation-Gasdynamic Coupling Behind Reflected Shock Waves in Air," presented at the 12th International Congress on Applied Mechanics held at Stanford University, California, August 26-31, 1968.

5. Nerem, R. M., "Research on Problems of High Enthalpy Flows," Aerospace Research Laboratories Report ARL 69-0145, September 1969.

6. Knott, P. R., Carlson, L. A., and Nerem, R. M., "A Further Note on Shock Tube Measurements of End-Wall Radiative Heat Transfer in Air," AIAA Journal, Vol. 7, No. 11, Nov. 1969, 2170-2172.

7. Nerem, R. M. and Stickford, G. H., "Shock Tube Studies of Equilibrium Radiation," AIAA Journal, Vol. 3, No. 6, June 1965, 1011-1018.

8. Wilson, K. H., Lockheed Palo Alto Research Laboratory, Private Communication, 1967.

9. Anderson, Jr., J. D., "Radiative Transfer Effects on the Flowfield and Heat Transfer Behind a Reflected Shock Wave in Air," Physics of Fluids, Vol. 10, No. 8, August 1967, 1785-1793.

10. Hanson, C. F., "Approximations for the Thermodynamic and Transport Properties of High-Temperature Air," NASA TR R-50, 1959.

11. Viegas, J. R. and Howe, J. T., "Thermodynamic and Transport Property Correlation Formulas for Equilibrium Air from 1,000°K to 15,000°K," NASA TN D-1429, October 1962.

12. Carlson, L. A., "Radiative Transfer, Chemical Nonequilibrium, and Two-Temperature Effects Behind a Reflected Shock Wave in Nitrogen," Ph. D. Dissertation, The Ohio State University, Columbus, Ohio, 1969.

13. Carlson, L. A., "Radiative-Gasdynamic Coupling, Two-Temperature, and Chemical Nonequilibrium Effects Behind Reflected Shock Waves," presented at the American Physical Society Fluid Dynamics Division Meeting, Norman, Oklahoma, November 24-26, 1969.

14. Carlson, L. A., "Expressions for the Exchange of Energy and Momentum Between Gases at Different Temperatures and Velocities," Physics of Fluids, Vol. 13, No. 7, July 1970, 1869-1870.

15. Carlson, L. A., "Radiative-Gasdynamic Coupling and Nonequilibrium Effects Behind Reflected Shock Waves," AIAA Journal, Vol. 9, No. 5, May 1971, 858-865 (also presented at AIAA Third Fluid and Plasma Daynamics Conference, Los Angeles, Calif., June 29-July 1, 1970 as AIAA Paper No. 70-774).

16. Hay, G. D., "An Approximate Small-Time Solution for a Transparent Radiating Gas Behind a Reflected Shock Wave," M. Sc. Thesis, The Ohio State University, Columbus, Ohio, 1968.

17. Lee, J. D., and Nerem, R. M., "Test Duration Measurements in a Shock Tube Having an Arc-Heated Driver," The Ohio State University Lab Report No. 1021-18, June 15, 1962.

18. Graber, B., and Nerem, R. M., "Test Duration Measurements in an Arc-Driven Hypervelocity Shock Tube," The Ohio State University, Aerodynamics Laboratory Report No. 1573-2, October 1963.

19. Golobic, R. A. and Nerem, R. M., "Shock Tube Studies of Radiative Transfer Effects in Air and Xenon," presented at NASA Langley Research Symposium on Hypervelocity Radiating Flow Fields for Earth and Planetary Entries, held at Hampton, Va., Jan. 22-23, 1971.

20. Nerem, R. M., Golobic, R. A., and Bader, J. B., "Laboratory Studies of Radiative Transfer Effects in Shock-Heated Gases," Shock Tube Research, Proceedings of the Eighth International Shock Tube Symposium, held July 5-8, 1971, Chapman and Hall, London, pp. 19/1-19/19.

21. Nerem, R. M. and Stickford, G. H., "A Thin Film Radiative Heat Transfer Gage," AIAA Journal, Vol. 6, No. 9, September 1968, 1741-1747.

22. Golobic, R. A. and Nerem, R. M., "Shock Tube Measurements of End-Wall Radiative Heat Transfer in Air," AIAA Journal, Vol. 6, No. 9, Sept. 1968, 1741-1746.

23. Rose, P. H., "Development of the Calorimeter Heat Transfer Gauge for Use in Shock Tubes," Avco-Everett Research Laboratory RR 17, February 1958.

24. Camac, M. and Feinberg, R. M., "High-Speed Infrared Bolometer," Avco-Everett Research Laboratory Report RR 120, March 1962.

25. Nerem, R. M. and Foley, W., "Studies of Strong Shock Waves in Air and Xenon: A Comparison Between Theory and Experiment," presented at Jet Propulsion Laboratory Symposium on Hypervelocity Radiating Flow Fields for Planetary Entries, held at Pasadena, Calif., Jan. 14-15, 1972.

26. Strehlow, R. A., and Cohen, A., "Limitations of the Reflected Shock Technique for Studying Fast Chemical Reactions and Its Application to the Observation of Relaxation in Nitrogen and Oxygen," J. Chem. Physics, Vol. 30, No. 1, 1959, 257-265.

27. Dyner, H. B., "Density Variation Due to Reflected Shock Boundary Layer Interaction," Physics of Fluids, Vol. 9, No. 5, 1966, 879-892.

28. Page, W. A., Compton, D. L., Borucki, W. J., Ciffone, D. L., and Cooper, D. M., "Radiative Transport in Inviscid Nonadiabatic Stagnation Region Shock Layers," AIAA Paper No. 68-784, presented at the AIAA Plasma and Fluid Dynamics Conference, Los Angeles, Calif., June 1968.

APPENDIX

PUBLICATIONS RESULTING FROM EFFORT ON GRANT

Theses, Journal Publications, and Proceedings

1. Carlson, L. A., "Radiative Transfer, Chemical Nonequilibrium, and Two-Temperature Effects Behind a Reflected Shock Wave in Nitrogen," Ph. D. Dissertation, The Ohio State University, Columbus, Ohio, 1969.

2. Carlson, L. A., "Expressions for the Exchange of Energy and Momentum Between Gases at Different Temperatures and Velocities," Physics of Fluids, Vol. 13, No. 7, July 1970, 1869-1870.

3. Carlson, L. A., "Radiative-Gasdynamic Coupling and Nonequilibrium Effects Behind Reflected Shock Waves," AIAA Journal, Vol. 9, No. 5, May 1971, 858-865.

4. Nerem, R. M., Golobic, R. A., and Bader, J. B., "Laboratory Studies of Radiative Transfer Effects in Shock-Heated Gases," Shock Tube Research, Proceedings of the Eighth International Shock Tube Symposium, held July 5-8, 1971, Chapman and Hall, London, 19/1-19/19.

5. Nerem, R. M., Bader, J. B., and Prior, R. C., "Radiative Transfer Effects Behind Reflected Shock Waves in Air," to be submitted for publication.

Symposium Presentations

1. Carlson, L. A., "Radiative-Gasdynamic Coupling, Two-Temperature, and Chemical Nonequilibrium Effects Behind Reflected Shock Waves," presented at the American Physica Society Fluid Dynamics Division Meeting, Norman, Oklahoma, November 24-26, 1969.

2. Carlson, L. A., "Radiative-Gasdynamic Coupling and Nonequilibrium Effects Behind Reflected Shock Waves," presented at AIAA Third Fluid and Plasma Dynamics Conference, Los Angeles, Calif., June 29-July 1, 1970 as AIAA Paper No. 70-774.

3. Golobic, R. A. and Nerem, R. M., "Shock Tube Studies of Radiative Transfer Effects in Air and Xenon," presented at NASA Langley Research Symposium on Hypervelocity Radiating Flow Fields for Earth and Planetary Entries, held at Hampton, Va., Jan. 22-23, 1971.

4. Nerem, R. M., Golobic, R. A., and Bader, J. B., "Laboratory Studies of Radiative Transfer Effects in Shock-Heated Gases," presented at the Eighth International Shock Tube Symposium, July 5-8, 1971, London.

5. Nerem, R. M. and Foley, W., "Studies of Strong Shock Waves in Air and Xenon: A Comparison Between Theory and Experiments," presented at Jet Propulsion Laboratory Symposium on Hypervelocity Radiating Flow Fields for Planetary Entries, held at Pasadena, Calif., Jan. 14-15, 1972.